Ivermectin action on glutamate- and GABA-gated chloride channels

(グルタミン酸およびGABA作動性クロルイオンチャネルに対する

イベルメクチンの作用**)**

Toshinori Fuse

布施　利紀

2017

Table of contents

Abbreviations

Chloramine-T: sodium *p*-toluenesulfonchloramide
DCC: *N,N*-dicyclohexylcarbodiimide
DDM: *n*-dodecyl-β-D-maltopyranoside
DIPEA: *N,N*-diisopropylethylamine
DMAP: 4-(dimethylamino)pyridine
DMF: *N,N*-dimethylformamide
DMSO: dimethyl sulfoxide
EC_x: x-percent effective concentration
EDC: 1-ethyl-3-(3-dimethylaminopropyl)carbodiimide hydrochloride
ESI: electrospray ionization
GABA: γ-aminobutyric acid
GABACl: GABA-gated chloride channel
GABAR: GABA receptor
Glu: L-glutamic acid
GluCl: L-glutamate-gated chloride channel
GluCl: GluCl subunit gene
GlyR: glycine receptor, glycine-gated chloride channel
Hco-AVR-14B: GluCl composed of AVR-14B subunits from *Haemonchus contortus*
HEPES: 4-(2-hydroxyethyl)-1-piperazineethanesulfonic acid
HOBt: 1-hydroxybenzotriazole
HRMS: high resolution mass spectroscopy
IC_{50}: fifty-percent inhibitory concentration
IVM: ivermectin
$IVMPO_4$: ivermectin 4''-*O*-phosphate
ML: macrocyclic lactone
MLM: milbemycin
nAChR: nicotinic acetylcholine receptor, acetylcholine-gated cation channel
NMR: nuclear magnetic resonance spectroscopy
$P2X_4R$: P2X purinoceptor 4, $P2X_4$ ATP-gated cation channel
PP: photoreactive probes
Rdl: Rdl subunit gene
SDS: sodium dodecyl sulfate

SEM: standard error of the mean
SOS: standard oocyte solution
TBDMS: *tert*-butyldimethylsilyl
THF: tetrahydrofuran
TLC: thin layer chromatography
Troc: trichloroethoxycarbonyl
UV: ultraviolet

Chapter 1

Introduction

Neurotransmitters

Neurotransmitters are small signaling molecules that are released from the terminal of neurons to transmit signals to neighbouring neurons in the synapse, and these chemicals change the electrical state of postsynaptic neurons by binding to ionotropic neurotransmitter receptors. The neurotransmitter receptors are responsible for fast synaptic transmission, and these transmissions result in excitation or inhibition in the central nervous system. Excitatory neurotransmitters, including acetylcholine, L-glutamic acid (Glu) (Fig. 1), and serotonin, cause depolarization in the cell by opening cation ion channels in mammals, and inhibitory neurotransmitters, including γ-aminobutyric acid (GABA) (Fig. 1) and glycine, cause hyperpolarization by opening anion channels for suppressing cell excitability. Therefore, neurotransmitters play an important role in controlling neuronal excitation and inhibition.

GABA, Glu, and their nervous system functions

GABA, which was first isolated from the brain (Awapara et al., 1950), is a major inhibitory neurotransmitter in the nervous system of vertebrates and invertebrates. Glu exerts both excitatory and inhibitory effects on neurotransmission by acting at different types of ionotropic receptors in invertebrates. Ionotropic GABA receptors and the inhibitory Glu receptors belong to the Cys-loop receptor family. The Cys-loop receptors are ligand-gated ion channels (LGICs), and therefore GABA and Glu receptors of this type are referred to as GABA-gated chloride channels (GABACls) and Glu-gated chloride channels (GluCls), respectively (Ozoe, 2013; Smart and Paoletti, 2012). GABACls and GluCls are activated by the agonists GABA and Glu, respectively, to enhance chloride ion permeability thorough the channels, which causes hyperpolarization in the postsynaptic neuron. GABACls and GluCls show differential distribution in the nervous system of insects (Démares et al., 2013; Harrison et al, 1996; Kita et al., 2013) and play distinct roles in a variety of physiological processes (Liu and Wilson, 2013; Ozoe, 2013).

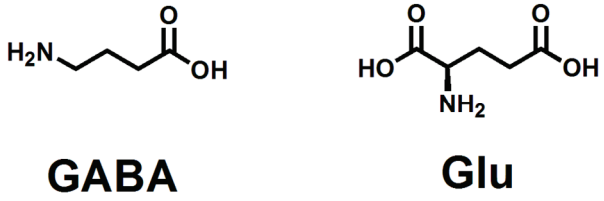

Fig. 1. Structures of the neurotransmitters GABA and Glu.

Structures of LGICs

LGICs including GABACls and GluCls are composed of five homologous subunits, each having an N-terminal extracellular domain containing inner and outer β-sheets, a C-terminal channel domain containing four α-helical transmembrane segments (TM1 to 4), and intracellular loops connecting TM1 to TM2 and TM3 to TM4 (Fig. 2A, B). The second transmembrane segment (TM2) contributes to the lining of the channel pore (Horenstein et al., 2001; Miller and Aricescu, 2014; Ozoe, 2013). There is a repertoire of 19 subunits, such as α, β, and γ subunits, in mammals, five of which are assembled to form a homo- or hetero-pentamer (Olsen and Sieghart, 2008). The orthosteric agonist-binding site is located at the subunit interface of the extracellular domains. Invertebrate Cys-loop ligand-gated ion channels have been objects of interest as targets of anthelmintics, acaricides, and insecticides.

Insect GluCls and GABACls as targets for insecticides and parasiticides

GluCls are anionic channels expressed only in the membranes of invertebrate nerve and muscle cells (Cleland, 1996). The two functional cDNAs encoding α and β subunits of GluCls were first cloned from *Caenorhabditis elegans* (Cully et al., 1994).

Insect GluCls are also homo-pentamers encoded by a single gene and its paralogs. An X-ray crystallography of the *C. elegans* GluCl revealed the three-dimensional structure, location of the Glu-, picrotoxin-, and IVM-binding sites, and gating mechanism (Hibbs and Gouaex, 2011; Althoff et al., 2014). Insect and nematode GluCls are the targets of insecticidal/anthelmintic macrocyclic lactones (MLs) such as avermectins (AVMs) (Raymond and Sattelle, 2002). There is solid evidence that the action of MLs on GluCls causes the paralysis and the death of parasitic nematodes (Arena et al., 1995; Dent et al., 2000; Glendinning, 2011).

Insect GABACls are anionic channels, and widely distributed in the insect nervous systems. The insect GABACl subunit (termed as Rdl) is encoded by a single gene *Rdl*

and its paralogs (ffrench-Constant et al., 1991; Remnant et al., 2013).

Insect GABACls are the important targets of insecticides/ectoparasiticides, such as phenylpyrazoles (e.g., fipronil), isoxazolines (e.g., fluralaner, fluxametamide, afoxolaner, sarolaner), and benzamides (e.g., broflanilide) (Buckingham et al., 2005; McTier et al., 2016; Nakao et al., 2016; Ozoe et al., 2010; Shoop et al., 2014). Benzodiazepins and bicuculline, important ligands that showed act as modulators and a competitive antagonist, respectively, in mammalian $GABA_A$ receptors, have no effect on insect GABACls.

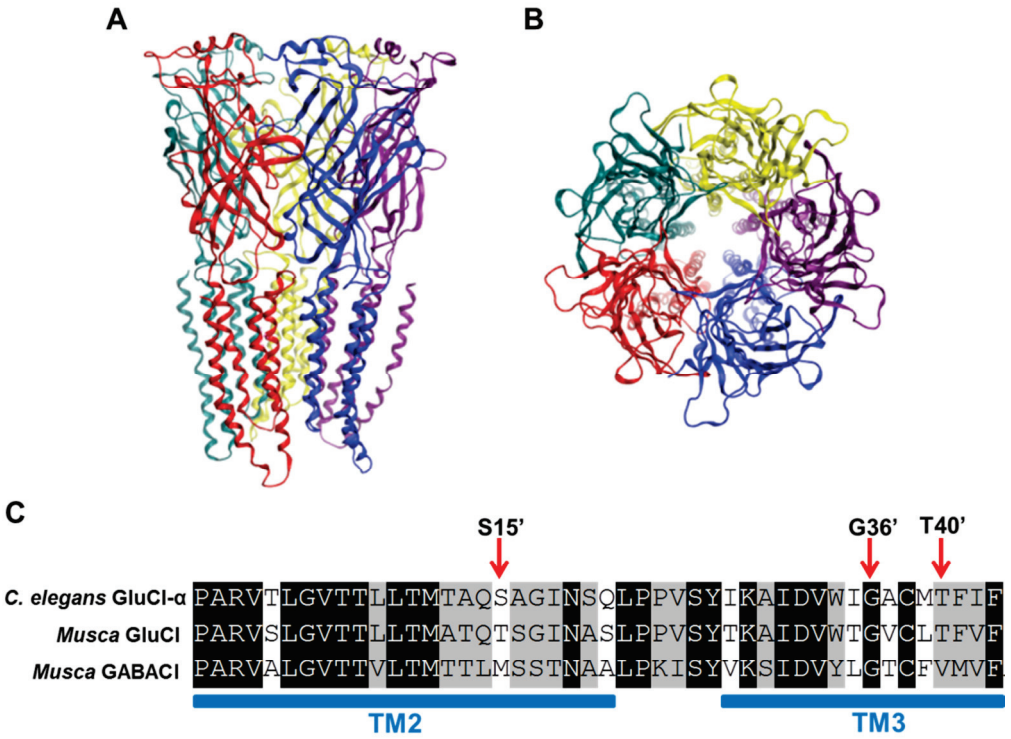

Fig. 2. Structure of the *Musca domestica* GluCl and sequence comparison. A homology model was constructed using the X-ray crystal structure (PDB; 3RIF) of *Caenorhabditis elegans* GluCl-α subunit as a template. (A) Side view of the *Musca* GluCl. (B) Top view of the *Musca* GluCl. (C) Alignment of amino acid sequences of the TM2 and the TM3 regions of *C. elegans* GluCl-α (accession No. U14524), *Musca* GluCl A (accession No. AB177546), and *Musca* Rdl_{ac} (accession Nos. AB177547, AB824728, AB824729) subunits. Conserved residues in three sequences are highlighted by white letters against the black background, and amino acids conserved in two sequences are shaded. Prime numbers are based on Charnet et al., 1990.

Avermectins and ivermectin

Avermectins (AVMs), which are antibiotics that are produced by the actinomycete *Streptomyces avermitilis*, contain a 16-membered macrocyclic lactone ring, a spiroketal unit, a hexahydrobenzofuran unit, and a dioleandrosyl group in their structure (Fig. 3). Ivermectin (IVM) is synthesized by the catalytic hydrogenation of AVM B_{1a} and B_{1b} (abamectin) at the C22-C23 double bond (Fig. 3) (Burg et al., 1979).

AVMs and IVM have a broad pharmacological spectrum against a wide variety of endo- and ectoparasites including nematodes and arthropods in humans and livestock (Lasota and Dybas, 1991; Õmura and Crump, 2004; Shoop et al., 1995). The main biological target of AVMs and IVM is GluCl, but it was reported that IVM modulates various ion channels such as invertebrate GABACls, vertebrate type-A GABACls ($GABA_A$Rs), α7 nicotinic acetylcholine-gated cation channels (nAChRs), $P2X_4$ ATP-gated cation channels ($P2X_4$Rs), and glycine-gated chloride channels (GlyRs) (Adelsberger et al., 2000; Khakh et al., 1999; Krause et al., 1998; Krůšek and Zemková, 1994; Lee et al., 2014; Nakao et al., 2015; Shan et al., 2001; Sigel and Baur, 1987). AVMs and IVM exhibit different actions, including the activation of GABACls and the potentiation and inhibition of GABA-induced currents in GABACls, the activation of GlyRs, and the potentiation of agonist-induced currents in nAChRs and $P2X_4$Rs. A conserved glycine residue in the third transmembrane segment (TM3) of GluCl subunits is extremely important for the actions of AVMs because the G323D (G36'D) and G326E (G36'E) mutation in TM3 confers a high level of resistance of *Tetranychus urticae* to abamectin (Fig. 2C) (Kwon et al., 2010; Dermauw et al., 2012). The equivalent Gly residue is likely involved in IVM binding to various Cys-loop receptors (Lynagh and Lynch, 2010). X-ray crystallographic analysis showed that IVM B_{1a} binds at the transmembrane interface crevice between principal (+) and complementary (-) subunits in the *Caenorhabditis elegans* GluCl-α channel (Hibbs and Gouaux, 2011). Site-directed mutagenesis studies showed that milbemycin (MLM) A4, an analog of AVMs, (Fig. 3) binds to both the transmembrane domain and extracellular domain in the *Haemonchus contortus* GluCl containing AVR-14B subunits (Yamaguchi et al., 2012).

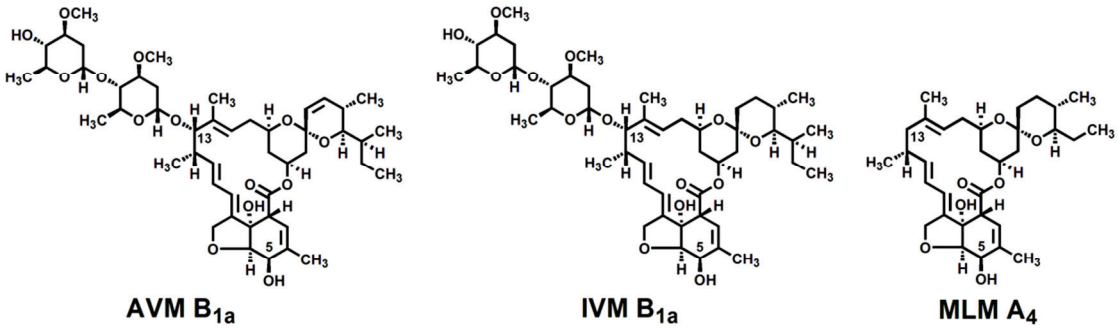

Fig. 3. Structures of AVM B_{1a}, IVM B_{1a}, and MLM A_4.

The objectives of the study

The IVM- and MLM-binding sites in GluCls were identified by crystallographical and molecular biological techniques. However, identification of the IVM-binding site by chemical means has yet to be achieved. To address this important issue regarding the macrolide-binding allosteric site, we synthesized three photoreactive probes (PPs) in which the disaccharide moiety of IVM B_{1a} was replaced by different photoreactive substituents, and photoaffinity labeling experiments were conducted using the synthesized radiolabeled IVM probe (Chapter 2).

IVM exhibits various actions on ion channels. In the present study, electrophysiological analyses were performed to clarify what type of action of IVM B_{1a} in *Musca* GluCls or GABACls plays primary roles in the manifestation of their insecticidal effects (Chapter 3).

Chapter 2

Synthesis of photoreactive IVM analogs for identification of the IVM-binding site

Introduction

Molecular cloning and functional expression studies revealed that macrolides such as IVM potentiate the Glu response of GluCls and/or activate GluCls to induce persistent inward chloride currents by binding to a site distinct from the orthosteric site (Cully et al., 1994, 1996). Thus, these macrolides act as positive allosteric modulators of GluCls with high affinity and irreversibility. Recently, the X-ray crystal structure of a *Caenorhabditis elegans* GluCl was solved as a complex with IVM B_{1a} bound in the transmembrane domain. In contrast, site-directed mutagenesis studies using a GluCl containing AVR-14B (also known by α3B) subunits from the parasitic nematode *Haemonchus contortus* (hereafter Hco-AVR-14B) suggested that MLM A4, an analog of IVM, may interact with the interface between the extracellular domain and the transmembrane domain. However, identification of the macrolide-binding site by chemical means has yet to be achieved. In this chapter, to address this important issue regarding the macrolide-binding allosteric site, I describe the synthesis of three photoreactive probes (PPs) in which the disaccharide moiety of IVM B_{1a} was replaced by different photoreactive substituents. This chapter demonstrates that these PPs possess pharmacological properties suitable for labeling the IVM-binding site in GluCls and that a future direction of the synthesis of improved probes was proposed, although my attempt to label Hco-AVR-14B-GluCls failed using these probes.

Materials and Methods

Synthesis of PPs

General methods and chemicals

^{1}H NMR spectra were recorded on a JEOL JNM-A 400 spectrometer. Chemical

shifts (δ) are reported in ppm relative to tetramethylsilane as the internal standard. Mass spectra were recorded on a Waters LCT Premier XE mass spectrometer. Melting points were determined using a Yanaco MP-500D apparatus and are uncorrected. IVM ($B_{1a} \geq 90$, $B_{1b} \leq 5\%$) was purchased from Sigma-Aldrich (St. Louis, MO), and [24,25-^{3}H]IVM B_{1a} (50 Ci/mmol) and [^{125}I]NaI (17.4 mCi/μg) were purchased from American Radiolabeled Chemicals. Chloramine-T trihydrate and other general chemicals were purchased from Wako Pure Chemical Industries, unless otherwise noted.

*IVM B_{1a} monosaccharide (**1**)*

IVM B_{1a} (200 mg, 0.229 mmol) was added to a solution of 1% sulfuric acid in MeOH (20 ml) and stirred at room temperature for 3 h (Mrozik et al., 1982). After CH_2Cl_2 (100 ml) was added to the reaction mixture, the solution was successively washed with a saturated $NaHCO_3$ solution (30 ml) and water (30 ml), dried over anhydrous Na_2SO_4, and then evaporated in vacuo. The residue was purified by silica gel column chromatography (CH_2Cl_2:THF, 20:1) to yield 128 mg (73%) of **1** as a white solid. ^{1}H NMR ($CDCl_3$) δ 5.87 (1H, dd, J = 10.0, 2.4 Hz, H_9), 5.68-5.79 (2H, m, H_{10}, H_{11}), 5.43 (1H, s, H_3), 5.31-5.37 (1H, m, H_{19}), 4.99 (1H, d, J = 9.0 Hz, H_{15}), 4.82 (1H, d, J = 3.4 Hz, $H_{1'}$), 4.70 (1H, dd, J = 14.0, 2.4 Hz, H_{8a}), 4.65 (1H, dd, J = 14.0, 2.4 Hz, H_{8a}), 4.29 (1H, d, J = 5.4 Hz, H_5), 4.17 (1H, br s, C_7-OH), 3.97 (1H, s, H_{13}), 3.96 (1H, d, J = 6.1 Hz, H_6), 3.83-3.90 (1H, m, $H_{5'}$), 3.65-3.76 (1H, m, H_{17}), 3.53-3.60 (1H, m, $H_{3'}$), 3.49 (3H, s, $C_{3'}$-OCH_3), 3.28 (1H, dd, J = 4.6, 2.2 Hz, H_2), 3.22 (1H, d, J = 7.6 Hz, H_{25}), 3.16 (1H, t, J = 9.3 Hz, $H_{4'}$), 2.80 (1H, br s, C_5-OH), 2.50-2.54 (1H, m, H_{12}), 2.23-2.33 (3H, m, H_{16}, $H_{2'}$), 2.00 (1H, dd, J = 12.0, 3.4 Hz, H_{20}), 1.82-1.87 (4H, m, H_{4a}, $C_{4'}$-OH), 1.78 (1H, d, J = 13.0 Hz, H_{18}), 1.66 (1H, d, J = 12.0 Hz, H_{22}), 1.50 (3H, s, H_{14a}), 1.40-1.56 (8H, m, H_{22}, H_{23}, H_{24}, H_{26}, H_{27}, $H_{2'}$), 1.35 (1H, t, J = 12.0 Hz, H_{20}), 1.27 (3H, d, J = 6.1 Hz, $H_{6'}$) 1.15 (3H, d, J = 6.8 Hz, H_{12a}), 0.94 (3H, t, J = 7.3 Hz, H_{28}), 0.86 (3H, d, J = 6.8 Hz, H_{26a}), 0.81 (1H, d, J = 16.0 Hz, H_{18}), 0.79 (3H, d, J = 5.4 Hz, H_{24a}).

*5-O-(t-Butyldimethylsilyl)IVM B_{1a} monosaccharide (**2**)*

To a solution of **1** (547 mg, 0.748 mmol) in dry *N*,*N*-dimethylformamide (DMF; 6.7 ml) were added imidazole (311 mg, 4.57 mmol) and *t*-butyldimethylsilyl chloride (TBDMSCl; 338 mg, 2.24 mmol); the mixture was stirred at room temperature for 2 h (Blizzard et al., 1992). After Et_2O (40 ml) was added, the resulting mixture was washed three times with water (40 ml) and with brine (40 ml), dried over anhydrous Na_2SO_4,

and concentrated in vacuo. The residue was purified by silica gel column chromatography (CH_2Cl_2:THF, 49:1 to 19:1, gradient) to yield 481 mg (76%) of **2** as a white solid. ^{1}H NMR ($CDCl_3$) δ 5.81-5.84 (1H, m, H_9), 5.71-5.73 (2H, m, H_{10}, H_{11}), 5.33 (1H, s, H_3), 5.29-5.33 (1H, m, H_{19}), 4.98 (1H, d, *J* = 10.0 Hz, H_{15}), 4.82 (1H, d, *J* = 3.4 Hz, $H_{1'}$), 4.68 (1H, dd, *J* = 14.0, 2.4 Hz, H_{8a}), 4.58 (1H, dd, *J* = 14.0, 2.2 Hz, H_{8a}), 4.44 (1H, d, *J* = 4.9 Hz, H_5), 4.18 (1H, br s, C_7-OH), 3.96 (1H, br s, H_{13}), 3.83 (1H, m, $H_{5'}$), 3.82 (1H, d, *J* = 5.4 Hz, H_6), 3.64-3.70 (1H, m, H_{17}), 3.53 (1H, m, $H_{3'}$), 3.48 (3H, s, $C_{3'}$-OCH_3), 3.38 (1H, dd, *J* = 4.6, 2.2 Hz, H_2), 3.22 (1H, d, *J* = 7.8 Hz, H_{25}), 3.17 (1H, t, *J* = 9.3 Hz, $H_{4'}$), 2.50-2.55 (2H, m, H_{12}, $C_{4'}$-OH), 2.23-2.32 (3H, m, H_{16}, $H_{2'}$), 1.99 (1H, ddd, *J* = 12.0, 4.6, 1.5 Hz, H_{20}), 1.79 (3H, s, H_{4a}), 1.74-1.80 (1H, m, H_{18}), 1.66 (1H, d, *J* = 12.0 Hz, H_{22}), 1.51 (3H, s, H_{14a}), 1.39-1.60 (8H, m, H_{22}, H_{23}, H_{24}, H_{26}, H_{27}, $H_{2'}$), 1.35 (1H, t, *J* = 12.0 Hz, H_{20}), 1.27 (3H, d, *J* = 6.1 Hz, $H_{6'}$), 1.15 (3H, d, *J* = 6.8 Hz, H_{12a}), 0.94 (9H, s, $SiC(CH_3)_3$), 0.90-0.95 (3H, m, H_{28}), 0.86 (3H, d, *J* = 6.6 Hz, H_{26a}), 0.79 (3H, d, *J* = 5.6 Hz, H_{24a}), 0.78-0.95 (1H, m, H_{18}), 0.13 (6H, s, $Si(CH_3)_2$).

*4'-O-(4-Azidobenzoyl)-5-O-TBDMS-IVM B_{1a} monosaccharide (**3**)*

To a solution of 4-azidobenzoic acid (877 mg, 5.38 mmol) in dry CH_2Cl_2 (7 ml) were added triethylamine (0.755 ml, 5.43 mmol) and pivaloyl chloride (0.657 ml, 5.34 mmol); the mixture was stirred at 0 °C for 30 min in the dark. To the mixture were added a solution of **2** (454 mg, 0.537 mmol) in dry CH_2Cl_2 (3 ml), *N*,*N*-diisopropylethylamine (DIPEA; 0.925 ml, 5.60 mmol) and 4-(dimethylamino)pyridine (DMAP; 335 mg, 2.74 mmol). The mixture was stirred at room temperature for 19 h and poured into ice-cold water (20 ml). After EtOAc (40 ml) was added to the mixture, the resulting mixture was successively washed with water (40 ml) and brine (40 ml), dried over anhydrous Na_2SO_4, and evaporated in vacuo. The residue was purified by silica gel column chromatography (CH_2Cl_2:THF, 59:1) to yield 700 mg (quant.) of **3** as a yellow solid. ^{1}H NMR ($CDCl_3$) δ 8.09 (2H, ddd, *J* = 8.5, 2.2, 1.7 Hz, *o*-PhH), 7.10 (2H, ddd, 8.5, 2.2, 1.7 Hz, *m*-PhH), 5.85 (1H, d, *J* = 10.0 Hz, H_9), 5.70-5.80 (2H, m, H_{10}, H_{11}), 5.30-5.37 (2H, m, H_3, H_{19}), 5.01 (1H, d, *J* = 12.0 Hz, H_{15}), 4.92 (1H, t, *J* = 9.3 Hz, $H_{4'}$), 4.87 (1H, d, *J* = 3.4 Hz, $H_{1'}$), 4.69 (1H, dd, *J* = 14.0, 2.2 Hz, H_{8a}), 4.59 (1H, dd, *J* = 14.0, 2.2 Hz, H_{8a}), 4.44 (1H, d, *J* = 5.4 Hz, H_5), 4.25 (1H, br s, C_7-OH), 4.03 (1H, m, $H_{5'}$), 3.98 (1H, br s, H_{13}), 3.83 (1H, d, *J* = 5.4 Hz, H_6), 3.65-3.84 (2H, m, H_{17}, $H_{3'}$), 3.40 (3H, s, $C_{3'}$-OCH_3), 3.40-3.42 (1H, m, H_2), 3.22 (1H, d, *J* = 7.8 Hz, H_{25}), 2.55 (1H, t, *J* = 6.1 Hz, H_{12}), 2.24-2.33 (3H, m, H_{16}, $H_{2'}$), 1.99 (1H, dd, *J* = 12.0, 5.1 Hz, H_{20}), 1.80 (3H, s, H_{4a}), 1.76 (1H, dd, *J* = 13.0, 3.9 Hz, H_{18}), 1.73 (1H,

dd, J = 13.0, 3.9 Hz, $H_{2'}$), 1.66 (1H, d, J = 12.0 Hz, H_{22}), 1.53 (3H, s, H_{14a}), 1.41-1.58 (7H, m, H_{22}, H_{23}, H_{24}, H_{26}, H_{27}), 1.36 (1H, t, J = 12.0 Hz, H_{20}), 1.19 (6H, t, J = 6.1 Hz, $H_{6'}$, H_{12a}), 0.94 (9H, s, $SiC(CH_3)_3$), 0.94 (3H, t, J = 7.3 Hz, H_{28}), 0.85 (3H, d, J = 6.6 Hz, H_{26a}), 0.83 (1H, d, J = 13.0 Hz, H_{18}) 0.79 (3H, d, J = 5.6 Hz, H_{24a}), 0.13 (6H, s, $Si(CH_3)_2$).

*4'-O-(4-Azidobenzoyl)IVM B_{1a} monosaccharide (**PP1**)*

Hydrogen fluoride (HF)-pyridine (7:3) (0.25 ml) was added to a solution of **3** (55.2 mg, 55.7 μmol) in acetonitrile (2.5 ml); the mixture was stirred at room temperature for 4.5 h in the dark. The reaction mixture was poured into an ice-cold saturated $NaHCO_3$ solution (20 ml) and extracted with EtOAc (20 ml). The organic extracts were successively washed with water (20 ml) and brine (20 ml), dried over anhydrous Na_2SO_4, and concentrated in vacuo. The residue was purified by silica gel column chromatography (CH_2Cl_2:THF, 39:1 to 19:1, gradient) to yield 32.8 mg (67%) of **PP1** as a yellow solid, mp 142-144 °C. ^{1}H NMR ($CDCl_3$) δ 8.09 (2H, ddd, J = 8.8, 2.4, 2.0 Hz, *o*-PhH), 7.10 (2H, ddd, J = 8.8, 2.4, 2.0 Hz, *m*-PhH) 5.89 (1H, d, J = 10.0 Hz, H_9), 5.71-5.83 (2H, m, $H_{10, 11}$), 5.43 (1H, s, H_3), 5.33 (1H, m, H_{19}), 5.02 (1H, d, J = 8.3 Hz, H_{15}), 4.92 (1H, t, J = 9.3 Hz, $H_{4'}$), 4.87 (1H, d, J = 3.2 Hz, $H_{1'}$), 4.72 (1H, dd, J = 14.0, 2.4 Hz, H_{8a}), 4.67 (1H, dd, J = 14.0, 2.2 Hz, H_{8a}), 4.44 (1H, br s, H_5), 4.16 (1H, br s, C_7-OH), 4.04 (1H, m, $H_{5'}$), 3.99 (1H, br s, H_{13}), 3.98 (1H, d, J = 6.3 Hz, H_6), 3.77 (1H, m, $H_{3'}$), 3.66-3.73 (1H, m, H_{17}), 3.40 (3H, s, $C_{3'}$-OCH_3), 3.30 (1H, dd, J = 4.6, 2.2 Hz, H_2), 3.22 (1H, d, J = 7.3 Hz, H_{25}), 2.55 (1H, t, J = 6.6 Hz, H_{12}), 2.27-2.35 (4H, m, H_{16}, $H_{2'}$, C_5-OH), 1.98 (1H, dd, J = 12.0, 4.9 Hz, H_{20}), 1.88 (3H, s, H_{4a}), 1.71-1.78 (2H, m, H_{18}, $H_{2'}$), 1.66 (1H, d, J = 12.0 Hz, H_{22}), 1.52 (3H, s, H_{14a}), 1.41-1.57 (7H, m, H_{22}, H_{23}, H_{24}, H_{26}, H_{27}), 1.37 (1H, t, J = 12.0 Hz, H_{20}), 1.17-1.21 (6H, m, $H_{6'}$, H_{12a}), 0.94 (3H, t, J = 7.3 Hz, H_{28}), 0.86 (3H, d, J = 6.6 Hz, H_{26a}), 0.82 (1H, d, J = 12.0 Hz, H_{18}), 0.79 (3H, d, J = 5.6 Hz, H_{24a}). HRMS (ESI) m/z calcd for $C_{48}H_{65}N_3O_{12}$ ($[M + Na]^+$), 898.4466; found, 898.4456.

*IVM B_{1a} aglycone (**4**)*

IVM B_{1a} (503 mg, 0.574 mmol) was added to a solution of 10% sulfuric acid in MeOH (10 ml); the mixture was stirred at room temperature for 2 h. After CH_2Cl_2 (40 ml) was added to the reaction mixture, the solution was successively washed with a saturated $NaHCO_3$ solution (40 ml) and water (40 ml), dried over Na_2SO_4, and

concentrated in vacuo. The residue was purified by silica gel column chromatography (CH_2Cl_2:THF, 50:1 to 20:1 gradient) to yield 296 mg (88%) of **4** as a white solid. ^{1}H NMR ($CDCl_3$) δ 5.81-5.85 (1H, m, H_9), 5.68-5.79 (2H, m, H_{10}, H_{11}), 5.41 (1H, br s, H_3), 5.27-5.35 (2H, m, H_{15}, H_{19}), 4.70 (1H, dd, *J* = 14.4, 2.2 Hz, H_{8a}), 4.66 (1H, dd, *J* = 14.4, 2.2 Hz, H_{8a}), 4.28 (1H, br s, H_5), 4.08 (1H, s, C_7-OH), 4.01 (1H, br s, H_{13}), 3.97 (1H, d, *J* = 6.1 Hz, H_6), 3.64-3.72 (1H, m, H_{17}), 3.26 (1H, dd, *J* = 4.4, 2.2 Hz, H_2), 3.18 (1H, d, *J* = 7.6 Hz, H_{25}), 2.50-2.56 (1H, m, H_{12}), 2.24-2.37 (3H, m, H_{16}, C_5-OH), 1.98 (1H, ddd, *J* = 12.2, 4.9, 2.0 Hz, H_{20}), 1.84-1.88 (3H, m, H_{4a}), 1.75 (1H, dt, *J* = 12.4, 2.4 Hz, H_{18}), 1.64-1.67 (2H, m, H_{22}, C_{13}-OH), 1.53 (3H, s, H_{14a}), 1.33-1.55 (8H, m, H_{20}, H_{22}, H_{23}, H_{24}, H_{26}, H_{27}) , 1.30 (1H, t, *J* = 11.0 Hz, H_{20}), 1.18 (3H, d, *J* = 7.1 Hz, H_{12a}), 0.96 (3H, t, *J* = 7.3 Hz, H_{28}), 0.85 (3H, d, *J* = 6.8 Hz, H_{26a}), 0.80 (3H, d, *J* = 5.9 Hz, H_{24a}), 0.79 (1H, d, *J* = 10.7 Hz, H_{18}).

*5-O-TBDMS-IVM B_{1a} aglycone (**5**)*

Compound **5** was synthesized from **4** (246 mg, 0.420 mmol) using the same method as for **2**. The residue was purified by silica gel column chromatography (CH_2Cl_2:THF, 39:1) to yield 219 mg (74%) of **5** as a white solid. ^{1}H NMR ($CDCl_3$) δ 5.65-5.80 (3H, m, H_9, H_{10}, H_{11}), 5.23-5.34 (3H, m, H_3, H_{15}**,** H_{19}), 4.68 (1H, dd, *J* = 14.2, 2.0 Hz, H_{8a}), 4.58 (1H, dd, *J* = 14.2, 2.0 Hz, H_{8a}), 4.43-4.44 (1H, m, H_5), 4.09 (1H, br s, C_7-OH), 4.01 (1H, br s, H_{13}), 3.81 (1H, d, *J* = 5.6 Hz, H_6), 3.64-3.70 (1H, m, H_{17}), 3.35 (1H, dd, *J* = 4.6, 2.2 Hz, H_2), 3.19 (1H, d, *J* = 7.8 Hz, H_{25}), 2.50-2.55 (1H, m, H_{12}), 2.24-2.32 (2H, m, H_{16}), 2.00 (1H, dd, *J* = 12.0, 3.4 Hz, H_{20}), 1.79 (3H, s, H_{4a}), 1.74 (1H, dt, *J* = 12.2, 2.2 Hz, H_{18}), 1.26-1.67 (13H, m, H_{14a}, H_{20}, H_{22}, H_{23}, H_{24}, H_{26}, H_{27}, C_{13}-OH), 1.17 (3H, d, *J* = 7.1 Hz, H_{12a}), 0.82-0.98 (7H, m, H_{18}, H_{26a}, H_{28}), 0.93 (9H, s, $SiC(CH_3)_3$), 0.79 (3H, d, *J* = 5.6 Hz, H_{24a}), 0.13 (6H, s, $Si(CH_3)_2$).

*5-O-TBDMS-13-O-[3-(2,2,2-trichloroethoxycarbonylamino)propanoyl]IVM B_{1a} aglycone (**6**)*

Compound **6** was synthesized from **5** (211 mg, 0.301 mmol) and 2-(2,2,2-trichloro-ethoxycarbonyl)-β-alanine (Mrozik et al., 1982) (*N*-Troc-β-alanine; 490 mg, 3.01 mmol) using the same method as for **3**. The residue was purified by silica gel column chromatography (hexane:EtOAc, 5:1 to 3:1, gradient) to yield 175 mg (61%) of **6** as a white solid. ^{1}H NMR ($CDCl_3$) δ 5.62-5.84 (3H, m, H_9, H_{10}, H_{11}), 5.56 (1H, t, *J* = 6.3 Hz, NH), 5.25-5.33 (2H, m, H_3, H_{19}), 5.19 (1H, br s, H_{13}), 4.97 (1H, dd, *J* = 8.5, 6.3 Hz ,

H_{15}), 4.72 (2H, s, CCl_3-CH_2), 4.69 (1H, d, *J* = 14.9 Hz, H_{8a}), 4.58 (1H, d, *J* = 14.9 Hz, H_{8a}), 4.43-4.44 (1H, m, H_5), 4.20 (1H, br s, C_7-OH), 3.82 (1H, d, *J* = 5.4 Hz, H_6), 3.53-3.66 (3H, m, H_{17}, N-CH_2), 3.36 (1H, dd, *J* = 4.6, 2.4 Hz, H_2), 3.19 (1H, d, *J* = 7.8 Hz, H_{25}), 2.61-2.78 (3H, m, H_{12}, C-CH_2-CO_2), 2.21-2.29 (2H, m, H_{16}), 2.00 (1H, dd, *J* = 12.2, 3.9 Hz, H_{20}), 1.79 (3H, s, H_{4a}), 1.71 (1H, dt, *J* = 12.4, 2.2 Hz, H_{18}), 1.64 (1H, d, *J* = 12.2 Hz, H_{22}), 1.60 (3H, s, H_{14a}), 1.39-1.58 (7H, m, H_{22}, H_{23}, H_{24}, H_{26}, H_{27}), 1.33 (1H, t, *J* = 12.0 Hz, H_{20}), 1.03 (3H, d, *J* = 6.8 Hz, H_{12a}), 0.84-0.96 (7H, m, H_{18}, H_{26a}, H_{28}), 0.93 (9H, s, $SiC(CH_3)_3$), 0.79 (3H, d, *J* = 5.1 Hz, H_{24a}), 0.13 (6H, s, $Si(CH_3)_2$).

5-O-TBDMS-13-O-(3-aminopropanoyl)IVM B_{1a} aglycone (7)

To a solution of **6** (153 mg, 0.161 mmol) in dry THF (8 ml) were added water (10 µl), acetic acid (100 µl) and zinc powder (752 mg, 11.6 atom); the mixture was stirred at room temperature for 3 h. The mixture was filtered through Celite®, which was washed with EtOAc (30 ml). The filtrate was successively washed with water (30 ml) and brine (30 ml), dried over anhydrous Na_2SO_4, and concentrated in vacuo. The residue was purified by silica gel column chromatography (CH_2Cl_2:THF, 20:1, 10:1 to 5:1, gradient) to yield 102 mg (82%) of **7** as a yellow solid. ^{1}H NMR ($CDCl_3$) δ 5.64-5.86 (3H, m, H_9, H_{10}, H_{11}), 5.33 (1H, d, *J* = 1.7 Hz, H_3), 5.23-5.30 (1H, m, H_{19}), 5.20 (1H, br s, H_{13}), 5.01 (1H, dd, *J* = 10.0, 3.7 Hz, H_{15}), 4.68 (1H, dd, *J* = 14.4, 1.7 Hz, H_{8a}), 4.57 (1H, dd, *J* = 14.4, 1.7 Hz, H_{8a}), 4.44-4.45 (1H, m, H_5), 4.37 (2H, br s, C-NH_2, D_2O exchangeable), 3.82 (1H, d, *J* = 5.6 Hz, H_6), 3.61-3.68 (1H, m, H_{17}), 3.35 (1H, q, *J* = 2.2 Hz, H_2), 3.19 (3H, br d, *J* = 8.1 Hz, H_{25}, N-CH_2), 2.70-2.88 (2H, m, C-CH_2-CO_2), 2.61-2.69 (1H, m, H_{12}), 2.20-2.31 (2H, m, H_{16}), 2.01 (1H, dd, *J* = 12.2, 4.4 Hz, H_{20}), 1.79 (3H, s, H_{4a}), 1.72 (1H, dt, *J* = 12.0, 2.2 Hz, H_{18}), 1.64 (1H, d, *J* = 11.7 Hz, H_{22}), 1.59 (3H, s, H_{14a}), 1.38-1.54 (7H, m, H_{22}, H_{23}, H_{24}, H_{26}, H_{27}), 1.32 (1H, t, *J* = 12.0 Hz, H_{20}), 1.04 (3H, d, *J* = 7.1 Hz, H_{12a}), 0.83-0.97 (7H, m, H_{18}, H_{26a}, H_{28}), 0.93 (9H, s, $SiC(CH_3)_3$), 0.78 (3H, d, *J* = 5.6 Hz, H_{24a}), 0.13 (6H, s, $Si(CH_3)_2$).

*5-O-TBDMS-13-O-[3-(4-azidobenzoylamino)propanoyl]IVM B_{1a} aglycone (**8**)*

To a solution of **7** (40.1 mg, 51.9 µmol) in dry CH_2Cl_2 (2.5 ml) were added 4-azidobenzoic acid (15.2 mg, 93.4 µmol) and dicyclohexylcarbodiimide (DCC; 24.6 mg, 0.119 mmol); the mixture was stirred at room temperature for 15 h in the dark. The mixture was evaporated in vacuo, and the residue was purified by silica gel column chromatography (EtOAc:hexane, 3:1) to yield 47.6 mg (quant.) of **8** as a pale yellow

solid. ^{1}H NMR ($CDCl_3$) δ 7.75 (2H, dt, *J* = 8.8, 2.0 Hz, *o*-PhH), 7.06 (2H, dt, *J* = 8.8, 2.0 Hz, *m*-PhH), 6.84 (1H, t, *J* = 5.9 Hz, NH), 5.74-5.82 (2H, m, H_9, H_{11}), 5.65 (1H, ddd, *J* = 12.2, 9.8, 2.4 Hz, H_{10}), 5.32 (1H, d, *J* = 1.5 Hz, H_3), 5.24-5.29 (1H, m, H_{19}), 5.20 (1H, s, H_{13}), 4.97 (1H, dd, *J* = 9.3, 6.3 Hz, H_{15}), 4.68 (1H, d, *J* = 14.1 Hz, H_{8a}), 4.57 (1H, d, *J* = 14.1 Hz, H_{8a}), 4.43-4.44 (1H, m, H_5), 4.16 (1H, s, C_7-OH, D_2O exchangeable), 3.82 (1H, d, *J* = 5.9 Hz, H_6), 3.70-3.79 (2H, m, N-CH_2), 3.60 (1H, dd, *J* = 15.1, 9.8 Hz, H_{17}), 3.36 (1H, dd, *J* = 4.9, 2.4 Hz, H_2), 3.13 (1H, d, *J* = 7.3 Hz, H_{25}), 2.69-2.84 (2H, m, C-C$\underline{H_2}$-CO_2), 2.61-2.69 (1H, m, H_{12}), 2.17-2.30 (2H, m, H_{16}), 1.99 (1H, dd, *J* = 12.2, 4.9 Hz, H_{20}), 1.79 (3H, s, H_{4a}), 1.69 (1H, dt, *J* = 13.0, 2.4 Hz, H_{18}), 1.62-1.65 (1H, m, H_{22}), 1.60 (3H, s, H_{14a}), 1.44-1.55 (5H, m, H_{22}, H_{23}, H_{24}, H_{26}), 1.38-1.43 (2H, m, H_{27}), 1.33 (1H, t, *J* = 11.7 Hz, H_{20}), 1.02 (3H, d, *J* = 6.8 Hz, H_{12a}), 0.93 (9H, s, $SiC(CH_3)_3$), 0.91 (3H, t, *J* = 7.3 Hz, H_{28}), 0.83-0.86 (1H, m, H_{18}), 0.84 (3H, d, *J* = 6.8 Hz, H_{26a}), 0.77 (3H, d, *J* = 5.4 Hz, H_{24a}), 0.13 (6H, s, $Si(CH_3)_2$).

*13-O-[3-(4-Azidobenzoylamino)propanoyl]IVM B_{1a} aglycone (**PP2**)*

PP2 was synthesized from **8** (45.9 mg, 50 μmol) using the same method as for **PP1**. The residue was purified by silica gel column chromatography (EtOAc:hexane, 3:2) to yield 27.2 mg (68%) of **PP2** as a white solid, mp 135-138 °C. ^{1}H NMR ($CDCl_3$) δ 7.76 (2H, dt, *J* = 8.8, 2.0 Hz, *o*-PhH), 7.06 (2H, dt, *J* = 8.8, 2.0 Hz, *m*-PhH), 6.82 (1H, t, *J* = 5.9 Hz, NH), 5.75-5.87 (2H, m, H_9, H_{11}), 5.67 (1H, dd, *J* = 14.2, 9.8 Hz, H_{10}), 5.42 (1H, s, H_3), 5.28-5.36 (1H, m, H_{19}), 5.20 (1H, s, H_{13}), 4.98 (1H, t, *J* = 7.8 Hz, H_{15}), 4.70 (1H, dd, *J* = 14.4, 2.0 Hz, H_{8a}), 4.65 (1H, dd, *J* = 14.4, 2.0 Hz, H_{8a}), 4.30 (1H, t, *J* = 6.3 Hz, H_5), 4.12 (1H, s, C_7-OH, D_2O exchangeable), 3.97 (1H, d, *J* = 6.3 Hz, H_6), 3.66-3.83 (2H, m, N-CH_2), 3.57-3.64 (1H, m, H_{17}), 3.26 (1H, dd, *J* = 4.4, 2.2 Hz, H_2), 3.13 (1H, d, *J* = 7.3 Hz, H_{25}), 2.71-2.85 (2H, m, C-CH_2-CO_2), 2.63-2.68 (1H, m, H_{12}), 2.35 (1H, d, *J* = 8.1 Hz, C_5-OH, D_2O exchangeable), 2.22-2.30 (2H, m, H_{16}), 1.98 (1H, dd, *J* = 12.0, 3.4 Hz, H_{20}), 1.87 (3H, s, H_{4a}), 1.68-1.73 (1H, m, H_{18}), 1.64 (1H, d, *J* = 12.2 Hz, H_{22}), 1.59 (3H, s, H_{14a}), 1.46-1.56 (5H, m, H_{22}, H_{23}, H_{24}, H_{26}), 1.38-1.43 (2H, m, H_{27}), 1.32 (1H, t, *J* = 11.7 Hz, H_{20}), 1.03 (3H, d, *J* = 6.8 Hz, H_{12a}), 0.91 (3H, t, *J* = 7.3 Hz, H_{28}), 0.81-0.88 (1H, m, H_{18}), 0.84 (3H, d, *J* = 6.8 Hz, H_{26a}), 0.78 (3H, d, *J* = 5.4 Hz, H_{24a}). HRMS (ESI) *m*/*z* calcd for $C_{44}H_{56}N_4O_9Na$ ([M - H_2O + Na]$^+$), 807.3945; found, 807.3940.

*5-O-TBDMS-13-O-[3-[6-(Troc-amino)hexanoylamino]propanoyl]IVM B_{1a} aglycone (**9**)*

To a solution of **7** (103 mg, 0.134 mmol) in dry CH_2Cl_2 (5 ml) were added Troc-6-aminohexanoic acid (Lapatsanis et al., 1983) (55.0 mg, 0.180 mmol), 1-ethyl-3-(3-dimethylaminopropyl)carbodiimide (EDC) hydrochloride (106 mg, 0.554 mmol) and 1-hydroxybenzotriazole (HOBt) monohydrate (27.5 mg, 0.180 mmol); the mixture was stirred at room temperature for 16 h. The mixture was successively washed with a saturated $NaHCO_3$ solution (30 ml), water (30 ml) and brine (30 ml), dried over anhydrous Na_2SO_4, and concentrated in vacuo. The residue was purified by silica gel column chromatography (CH_2Cl_2:MeOH, 40:1) to yield 126 mg (89%) of **9** as a white solid. ^{1}H NMR ($CDCl_3$) δ 6.05 (1H, t, *J* = 5.4 Hz, NH), 5.61-5.83 (3H, m, H_9, H_{10}, H_{11}), 5.33 (1H, d, *J* = 1.5 Hz, H_3), 5.26-5.30 (1H, m, H_{19}), 5.19 (1H, br s, H_{13}), 5.08 (1H, br s, NH), 4.98 (1H, t, *J* = 8.3 Hz, H_{15}), 4.72 (2H, s, Cl_3-CH_2), 4.68 (1H, dd, *J* = 15.0 Hz, H_{8a}), 4.57 (1H, d, *J* = 15.0 Hz, H_{8a}), 4.43 (1H, br s, H_5), 4.15 (1H, s, C_7-OH), 3.82 (1H, d, *J* = 5.4 Hz, H_6), 3.50-3.67 (3H, m, H_{17}, N-CH_2-CCO_2), 3.36 (1H, q, *J* = 2.4 Hz, H_2), 3.13-3.37 (3H, m, H_{25}, N-CH_2-CCC), 2.57-2.73 (3H, m, H_{12}, C-CH_2-CO_2), 2.24-2.28 (2H, m, H_{16}), 2.16 (2H, t, *J* = 7.3 Hz, CH_2-CON), 2.00 (1H, dd, *J* = 12.0, 3.4 Hz, H_{20}), 1.79 (3H, s, H_{4a}), 1.26-1.71 (19H, m, H_{14a}, H_{18}, H_{20}, H_{22}, H_{23}, H_{24}, H_{26}, H_{27}, C-CH_2-CH_2-CH_2-C), 1.02 (3H, d, *J* = 6.8 Hz, H_{12a}), 0.83-1.00 (7H, m, H_{18}, H_{26a}, H_{28}), 0.93 (9H, s, $SiC(CH_3)_3$), 0.78 (3H, d, *J* = 5.4 Hz, H_{24a}), 0.13 (6H, s, $Si(CH_3)_2$).

*5-O-TBDMS-13-O-[3-(6-aminohexanoylamino)propanoyl]IVM B_{1a} aglycone (**10**)*

Compound **10** was synthesized from **9** (124 mg, 0.117 mmol) using the same method as for **7**. The residue was purified by silica gel column chromatography (CH_2Cl_2:MeOH, 20:1 to 5:1, gradient) to yield 34.7 mg (34%) of **10** as a yellow solid. ^{1}H NMR ($CDCl_3$) δ 6.65 (1H, t, *J* = 5.4 Hz, NH), 5.63-5.84 (3H, m, H_9, H_{10}, H_{11}), 5.33 (1H, br s, H_3), 5.20-5.30 (1H, m, H_{19}), 5.18 (1H, br s, H_{13}), 4.99 (1H, t, *J* = 8.3 Hz, H_{15}), 4.68 (1H, d, *J* = 15.0 Hz, H_{8a}), 4.58 (1H, d, *J* = 15.0 Hz, H_{8a}), 4.45 (1H, br s, H_5), 3.83 (1H, d, *J* = 5.9 Hz, H_6), 3.48-3.74 (5H, m, H_{17}, N-CH_2-CCC , N-CH_2-CCO_2), 3.35 (1H, d, *J* = 2.0 Hz, H_2), 3.19 (1H, d, *J* = 7.8 Hz, H_{25}), 3.01 (2H, t, *J* = 7.0 Hz, NH_2), 2.58-2.76 (3H, m, H_{12}, CH_2-CO_2), 2.19-2.28 (4H, m, H_{16}, CH_2-CON), 2.02 (1H, dd, *J* = 12.0, 4.4 Hz, H_{20}), 1.79 (3H, s, H_{4a}), 1.25-1.73 (19H, m, H_{14a}, H_{18}, H_{20}, H_{22}, H_{23}, H_{24}, H_{26}, H_{27}, C-CH_2-CH_2-CH_2-C), 1.03 (3H, d, *J* = 6.8 Hz, H_{12a}), 0.84-0.96 (7H, m, H_{18}, H_{26a}, H_{28}), 0.93 (9H, s, $SiC(CH_3)_3$), 0.78 (3H, d, *J* = 4.9 Hz, H_{24a}), 0.14 (6H, s, $Si(CH_3)_2$).

*5-O-(TBDMS-13-O-[3-[6-(4-azidobenzoylamino)hexanoylamino]propanoyl]IVM B_{1a} aglycone (**11**)*

To a solution of **10** (34.7 mg, 39.2 μmol) in dry CH_2Cl_2 (2 ml) were added 4-azidobenzoic acid (12.8 mg, 78.4 μmol), EDC (23.2 mg, 0.121 mmol) and HOBt monohydrate (6.50 mg, 42.5 μmol); the mixture was stirred at room temperature. After 28 h, additional EDC hydrochloride (25.7 mg, 0.134 mmol) was added; the mixture was stirred at room temperature for 22 h. The mixture was successively washed with a saturated $NaHCO_3$ solution (10 ml), water (10 ml) and brine (10 ml), dried over anhydrous Na_2SO_4, and concentrated in vacuo. The residue was purified by silica gel column chromatography (CH_2Cl_2:MeOH, 50:1 to 30:1, gradient) to yield 25.7 mg (64%) of **11** as a yellow solid. ^{1}H NMR ($CDCl_3$) δ 7.80 (2H, dd, *J* = 6.8, 2.0 Hz, *o*-PhH), 7.06 (2H, dd, *J* = 6.8, 2.0 Hz, m-PhH), 6.39 (1H, t, *J* = 5.4 Hz, NH), 6.10 (1H, t, *J* = 5.9 Hz, NH), 5.60-5.83 (3H, m, H_9, H_{10}, H_{11}), 5.33 (1H, br s, H_3), 5.24-5.33 (1H, m, H_{19}), 5.18 (1H, br s, H_{13}), 4.98 (1H, t, *J* = 7.8 Hz, H_{15}), 4.68 (1H, d, *J* = 15.0 Hz, H_{8a}), 4.57 (1H, d, *J* = 15.0 Hz, H_{8a}), 4.42 (1H, br s, H_5), 4.19 (1H, s, C_7-OH), 3.82 (1H,d, *J* = 5.9 Hz, H_6), 3.43-3.68 (5H, m, H_{17}, N-CH_2-CCC, N-CH_2-CCO_2), 3.36 (1H, d, *J* = 2.4 Hz, H_2), 3.18 (1H, d, *J* = 7.3 Hz, H_{25}), 2.61-2.73 (3H, m, H_{12}, CH_2-CO_2), 2.23-2.28 (2H, m, H_{16}), 2.18 (2H, t, *J* = 7.3 Hz, CH_2-CON), 2.00 (1H, dd, *J* = 12.0, 4.4 Hz, H_{20}), 1.79 (3H, s, H_{4a}), 1.25-1.76 (19H, m, H_{14a}, H_{18}, H_{20}, H_{22}, H_{23}, H_{24}, H_{26}, H_{27}, C-CH_2-CH_2-CH_2-C), 1.02 (3H, d, *J* = 6.8 Hz, H_{12a}), 0.80-0.96 (7H, m, $H_{18,}$ $H_{26a,}$ H_{28}), 0.93 (9H, s, $SiC(CH_3)_3$), 0.78 (3H, d, *J* = 4.9 Hz, H_{24a}), 0.14 (6H, s, $Si(CH_3)_2$).

*13-O-[3-[6-(4-Azidobenzoylamino)hexanoylamino]propanoyl]IVM B_{1a} aglycone (**PP3**)*

PP3 was synthesized from **11** (25.7 mg, 0.0249 mmol) using the same method as for **PP1**. The residue was purified by silica gel column chromatography (CH_2Cl_2:MeOH, 10:1) to yield 9.7 mg (42%) of **PP3** as a yellow solid, mp 109-111 °C. ^{1}H NMR ($CDCl_3$) δ 7.80 (2H, dd, *J* = 6.8, 2.0 Hz, *o*-PhH), 7.06 (2H, dd, *J* = 6.8, 1.5 Hz, *m*-PhH), 6.40 (1H, t, *J* = 5.4 Hz, NH), 6.10 (1H, t, *J* = 5.4 Hz, NH), 5.75-5.87 (2H, m, $H_{9,}$ H_{11}), 5.62-5.68 (1H, m, H_{10}), 5.42 (1H, br s, H_3), 5.28-5.37 (1H, m, H_{19}), 5.19 (1H, br s, H_{13}), 4.98 (1H, t, *J* = 7.8 Hz, H_{15}), 4.71 (1H, dd, *J* = 14.0, 2.0 Hz, H_{8a}), 4.65 (1H, dd, *J* = 14.0, 2.0 Hz, H_{8a}), 4.27 (1H, br s, H_5), 4.15 (1H, s, C_7-OH), 3.96 (1H, d, *J* = 5.9 Hz, H_6), 3.42-3.64 (5H, m, $H_{17,}$ N-CH_2-CCC, N-CH_2-CCO_2), 3.26 (1H, dd, *J* = 4.4, 2.4 Hz, H_2), 3.18 (1H, d, *J* = 7.8 Hz, H_{25}), 2.57-2.74 (3H, m, H_{12}, CH_2-CO_2), 2.23-2.36 (3H, m, H_{16}, C_5-OH), 2.18 (2H, t, *J* = 7.3 Hz, CH_2-CON), 1.97-2.07 (1H, m, H_{20}), 1.87 (3H, s, H_{4a}),

1.25-1.70 (19H, m, H_{14a}, H_{18}, H_{20}, H_{22}, H_{23}, H_{24}, H_{26}, H_{27}, C-CH_2-CH_2-CH_2-C), 1.03 (3H, d, J = 6.8 Hz, H_{12a}), 0.77-0.96 (10H, m, $H_{18,}$ $H_{24a,}$ $H_{26a,}$ H_{28}). HRMS (ESI) *m*/*z* calcd for $C_{50}H_{69}N_5O_{11}Na$ ($[M + Na]^+$), 938.4891; found, 938.4888.

*2-Hydroxyl-4-azidobenzoic acid (**12**)*

To a solution of 2-hydroxyl-4-aminobenzoic acid (1.00 g, 6.52 mmol) in HCl (15 ml) was added dropwise sodium nitrite (1.35 g, 19.6 mmol) in cold water (6.5 ml); the mixture was stirred at 0 °C for 30 min. Sodium azide (2.17 g, 33.7 mmol) in cold water (11 ml) was added dropwise to the mixture; the mixture was stirred at 0 °C for 3 h. The residue was filtrated, washed with cold water, and concentrated in vacuo to yield 617 mg (53%) of **12** as a yellow solid. ^{1}H-NMR (CD_3OD) δ 7.85 (1H, d, J=0.02 Hz, Ar-H), 6.58-6.61 (2H, m, Ar-H).

*Methyl-2-hydroxyl-4-azidobenzoate (**13**)*

A solution of **12** (602 mg, 3.35 mmol) and concentrated sulfuric acid (0.6 ml) in methanol (91 ml) was refluxed for 48 h. The mixture was neutralized with saturated NaOH solution, and the methanol was removed under reduced pressure. The residue was extracted with EtOAc, successively washed with $NaHCO_3$ solution (10 ml, three times), water (10 ml, two times), and brine (10 ml), dried over anhydrous Na_2SO_4, and concentrated in vacuo to yield 546 mg (84%) of **13** as a yellow solid. ^{1}H-NMR ($CDCl_3$) δ 11.0 (1H, s, Ar-OH), 7.80 (1H, d, J=0.02 Hz, Ar-H), 6.53-6.63 (2H, m, Ar-H), 3.94 (3H, s, CH_3).

*Methyl-2-hydroxyl-4-azido-5-iodobenzoate (**14**)*

A solution of **13** (546 mg, 2.83 mmol), sodium iodide (506 mg, 3.37 mmol), and chloramine-T trihydrate (950 mg, 3.37 mmol) in dry DMF (11 ml) was stirred at room temperature for 2 h. Water (20 ml) was added to the mixture, and the mixture was acidified with 1N HCl and extracted with EtOAc. The organic layer was washed with $Na_2S_2O_3$ solution (10 ml) and brine (10 ml), dried over anhydrous Na_2SO_4, concentrated in vacuo, and recrystallized from EtOAc to yield 332 mg (37%) of **14** as a yellow solid. ^{1}H-NMR ($CDCl_3$) δ 10.9 (1H, s, Ar-OH), 8.21 (1H, s, Ar-H), 6.76 (1H, s, Ar-H), 3.94 (3H, s, CH_3).

*2-Hydroxyl-4-azido-5-iodobenzoic acid (**15**)*

A solution of **14** (300 mg, 0.940 mmol) and LiOH-H_2O (77.3 mg, 1.84 mmol) in THF (3 ml) was stirred at 50 °C for 22 h. The mixture was acidified with 1N HCl to pH4, and extracted with EtOAc. The organic layer was washed with brine (10 ml), dried over anhydrous Na_2SO_4, and concentrated in vacuo. The residue was purified by silica gel column chromatography (CH_2Cl_2:THF, 5:1) to yield 299 mg (87%) of **15** as a yellow solid. ^{1}H NMR (CD_3OD) δ 8.10 (1H, s, Ar-H), 6.91 (1H, s, Ar-H)

*Succinimidyl 2-hydroxyl-4-azido-5-iodobenzoate (**16**)*

A solution of *N*-hydroxyl succinimide (39.6 mg, 0.344 mmol), EDC (67.6 mg, 0.352 mmol), and **15** (102 mg, 0.164 mmol) in acetone (7 ml) was stirred at room temperature for 20 h. The acetone was removed under reduced pressure and replaced CH_2Cl_2. The organic solution was washed with water (10 ml), dried over anhydrous Na_2SO_4, and concentrated in vacuo. Acetone (2 ml) was added to the mixture, and the suspension was filtrated and washed with acetone to yield 30.3 mg (22%) of **16** as a yellow solid. ^{1}H NMR ($CDCl_3$) δ 9.64 (1H, s, Ar-OH), 8.38 (1H, s, Ar-H), 6.82 (1H, s, Ar-H), 2.94 (4H, s, Su)

*5-O-TBDMS-13-O-[3-(2-hydroxyl-4-azido-5-iodobenzoyl)propanoyl]IVM B_{1a} aglycone (**17**)*

A solution of **7** (28.2 mg, 0.0370 mmol) and **16** (15.8 mg, 0.0393 mmol) in CH_2Cl_2 (2.3 ml) was stirred at room temperature for 25 h. The mixture was concentrated in vacuo and purified by silica gel column chromatography (hexane:EtOAc, 3:1) to yield 27.1 mg (69%) of **17** as a yellow solid. ^{1}H NMR ($CDCl_3$) δ 12.6 (1H, s, Ar-H), 7.65 (1H, s, Ar-H), 6.94 (1H, t, J = 5.9 Hz, NH), 6.75 (1H, s, Ar-H), 5.75-5.78 (2H, m, H_9, H_{11}), 5.62 (1H, ddd, J = 10.7, 10.2, 2.9 Hz, H_{10}), 5.32 (1H, s, H_3), 5.24-5.29 (1H, m, H_{19}), 5.21 (1H, s, H_{13}), 4.94 (1H, t, J = 7.8 Hz, H_{15}), 4.67 (1H, d, J = 14.6 Hz, H_{8a}), 4.56 (1H, d, J = 14.6 Hz, H_{8a}), 4.43 (1H, s, H_5), 4.18 (1H, s, C_7-OH), 3.81 (1H, d, J = 5.4 Hz, H_6), 3.71-3.80 (2H, m, N-CH_2), 3.55-3.70 (1H, m, H_{17}), 3.36 (1H, s, H_2), 3.13 (1H, d, J = 7.3 Hz, H_{25}), 2.68-2.82 (2H, m, C-C$\underline{H_2}$-CO_2), 2.65-2.68 (1H, m, H_{12}), 2.26-2.28 (2H, m, H_{16}), 1.97 (1H, dd, J = 12.0, 4.9 Hz, H_{20}), 1.79 (3H, s, H_{4a}), 1.17-1.79 (13H, m, H_{14a}, H_{18}, $H_{20,}$ H_{22}, H_{23}, H_{24}, H_{26}, H_{27}), 1.03 (3H, d, J = 6.8 Hz, H_{12a}), 0.93 (9H, s, $SiC(CH_3)_3$), 0.92 (3H, t, J = 2.9 Hz, H_{28}), 0.83-0.86 (1H, m, H_{18}), 0.83 (3H, d, J = 6.8 Hz, H_{26a}), 0.77

(3H, d, J = 5.4 Hz, H_{24a}), 0.13 (6H, s, $Si(CH_3)_2$).

*13-O-[3-(2-Hydroxyl-4-azido-5-iodobenzoyl)propanoyl]IVM B_{1a} aglycone (**IodoPP2**)*

IodoPP2 was synthesized from **17** (25.7 mg, 0.0249 mmol) using the same method as for **PP1**. The residue was purified by silica gel column chromatography (hexane:EtOAc, 2:3) to yield 19.1 mg (79%) of **IodoPP2** as a yellow solid. ^{1}H NMR ($CDCl_3$) δ 12.6 (1H, s, Ar-H), 7.67 (1H, s, Ar-H), 6.97 (1H, t, J = 6.0 Hz, NH), 6.75 (1H, s, Ar-H), 5.74-5.87 (2H, m, H_9, H_{11}), 5.64 (1H, dd, J = 10.2, 4.4 Hz, H_{10}), 5.42 (1H, s, H_3), 5.29-5.36 (1H, m, H_{19}), 5.22 (1H, s, H_{13}), 4.94 (1H, t, J = 7.8 Hz, H_{15}), 4.69 (1H, d, J = 12.2 Hz, H_{8a}), 4.64 (1H, d, J = 12.7 Hz, H_{8a}), 4.29 (1H, t, J = 3.9 Hz, H_5), 4.17 (1H, s, C_7-OH), 3.96 (1H, d, J = 6.3 Hz, H_6), 3.71-3.82 (2H, m, N-CH_2), 3.58-3.69 (1H, m, H_{17}), 3.26 (1H, s, H_2), 3.13 (1H, d, J = 7.8 Hz, H_{25}), 2.71-2.80 (2H, m, C-C$\underline{H_2}$-CO_2), 2.65-2.70 (1H, m, H_{12}), 2.24-2.38 (2H, m, H_{16}), 1.96-2.08 (1H, m, H_{20}), 1.87 (3H, s, H_{4a}), 1.19-1.72 (13H, m, H_{14a}, H_{18}, $H_{20,}$ H_{22}, H_{23}, H_{24}, H_{26}, H_{27}), 1.03 (3H, d, J = 6.8 Hz, H_{12a}), 0.82-0.92 (7H, m, $H_{18,}$ $H_{26a,}$ H_{28}), 0.78 (3H, d, J = 5.9 Hz, H_{24a}). ESI-MS m/z calcd for $C_{44}H_{56}IN_4O_{11}$ ($[M - H]^+$), 943.31; found, 943.3.

*13-O-[3-(2-Hydroxyl-4-azido-5-[^{125}I]iodobenzoyl)propanoyl]IVM B_{1a} aglycone (**[^{125}I]IodoPP2**)*

To a mixture of 1.0 mM **IodoPP2** in DMSO (25 µl) and 0.2 M aqueous NaH_2PO_4 (10 µl) in a 1.5 ml microtube was added [^{125}I]NaI (100 mCi/ml in NaOH aq., 5.0 µl). Subsequently, 5 mM aqueous chloramine-T trihydrate (5 µl) was added to the mixture, which was then incubated at room temperature for 5 min. The reaction was terminated with 1 M aqueous $N_2S_2O_5$ (25 µl), and the mixture was extracted with chloroform (100 µl) three times. The organic layer was purified by preparative TLC (EtOAc:hexane, 3:2). The radioactivity was measured by a γ-counting system (COBRA II5003, PerkinElmer). The radiochemical yield from the initially added [^{125}I]NaI was 60%, and the specific radioactivity was 1.2 Ci/mmol.

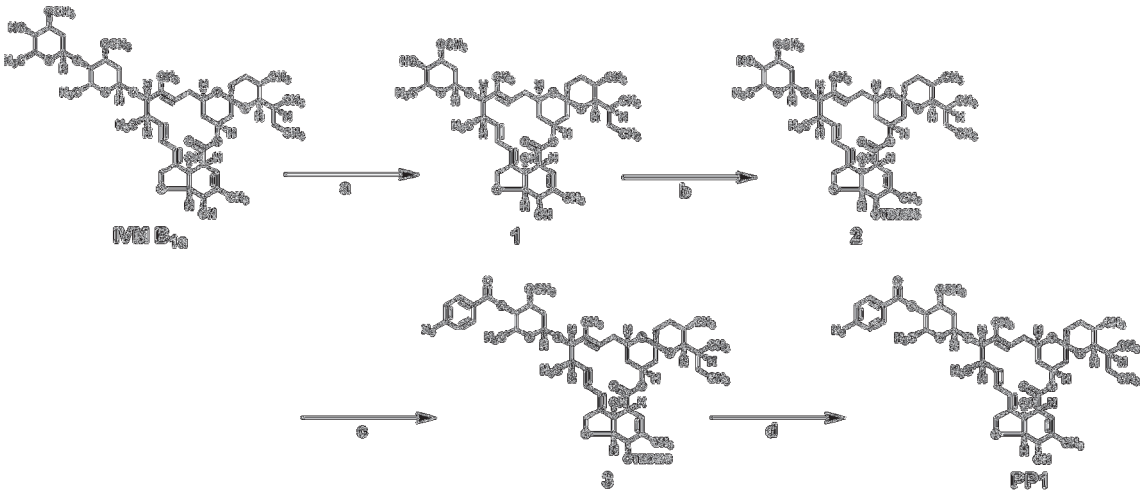

Scheme 1. Synthesis of PP1. Reagents: (a) 1% (v/v) H_2SO_4, MeOH; (b) TBDMSCl, imidazole, DMF; (c) 4-azidobenzoic acid, Et_3N, pivaloyl chloride, CH_2Cl_2, then **2**, DIPEA, DMAP; (d) HF-pyridine, acetonitrile.

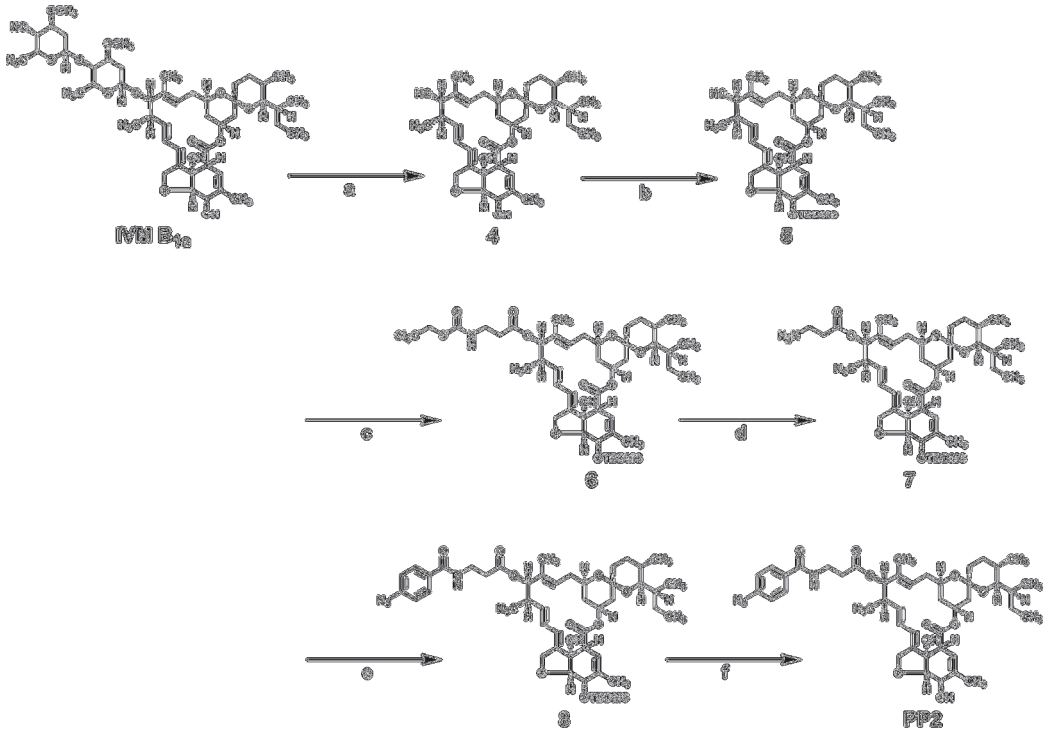

Scheme 2. Synthesis of PP2. Reagents: (a) 10% (v/v) H_2SO_4, MeOH; (b) TBDMSCl, imidazole, DMF; (c) *N*-Troc-β-alanine, Et_3N, pivaloyl chloride, CH_2Cl_2, then **5**, DIPEA, DMAP; (d) Zn, AcOH, H_2O, THF; (e) 4-azidobenzoic acid, DCC, CH_2Cl_2; (f) HF-pyridine, acetonitrile.

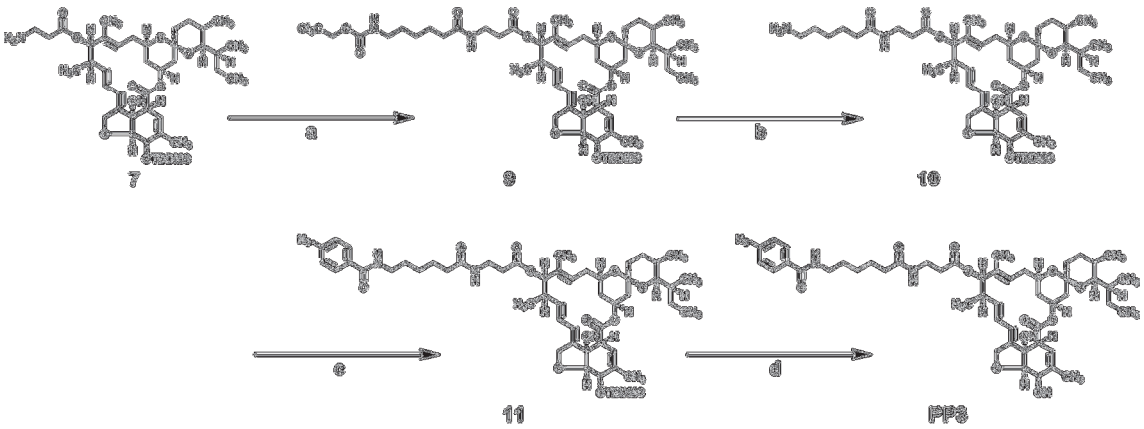

Scheme 3. Synthesis of PP3. Reagents: (a) *N*-Troc-6-aminohexanoic acid, EDC, HOBt, CH_2Cl_2; (b) Zn, AcOH, H_2O, THF; (c) 4-azidobenzoic acid, EDC, HOBt, CH_2Cl_2; (d) HF-pyridine, acetonitrile.

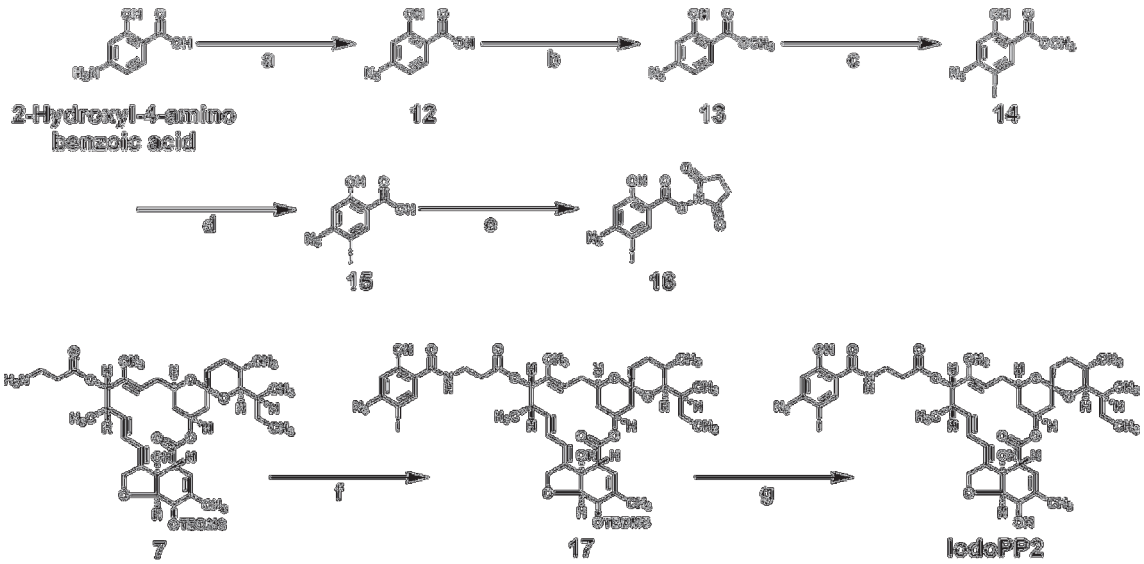

Scheme 4. Synthesis of IodoPP2. Reagents: (a) HCl, $NaNO_2$, then NaN_3; (b) H_2SO_4, MeOH; (c) NaI, chloramine-T trihydrate, DMF; (d) LiOH-H_2O, THF; (e) *N*-hydroxyl succinimide, EDC, acetone; (f) **16**, CH_2Cl_2; (g) HF-pyridine, acetonitrile.

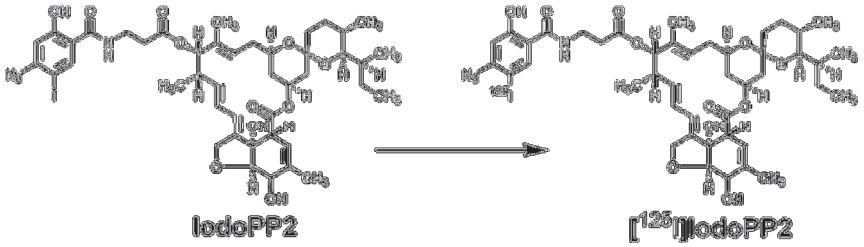

Scheme 5. Synthesis of [^{125}I]IodoPP2. Reagent: NaH_2PO_4, [^{125}I]NaI, chloramine-T trihydrate, DMSO.

Determination of the affinity of PPs for GluCls

Transient expression of GluCls in COS-1 cells

The plasmid vector pcDNA3 or pcDNA3.1(+) vector (Life Technologies, Grand Island, NY) was used to express GluCls in COS-1 cells. The pcDNA3 (pcDNA3-Hco-AVR-14B) inserted with cDNA (accession No. Y14234) encoding the Hco-AVR-14B (also known by α3B) subunit of *H. contortus* was available from an earlier study (Yamaguchi et al., 2012). The pcDNA3.1(+) construct of silkworm (*Bombyx mori*) GluCl cDNA was designed to produce a chimeric subunit (*Bombyx*/*D*-GluCl) in which the 11 C-terminal amino acids are from the *Drosophila* GluCl-α subunit (accession No. U58776) and the others are from the *Bombyx* GluCl exon 3c variant subunit (accession No. AB857001) to achieve efficient heterologous expression (Fig. 4). This plasmid vector was a gift from Professor Kazuhiko Matsuda, Kinki University. COS-1 cells (2.5×10^5 cells) were plated in Dulbecco's modified Eagle medium (Life Technologies) in a 35-mm φ dish, transfected with the plasmid vectors using Lipofectamine LTX™ (Life Technologies), and incubated in 5% CO_2 at 37 °C for 48 h.

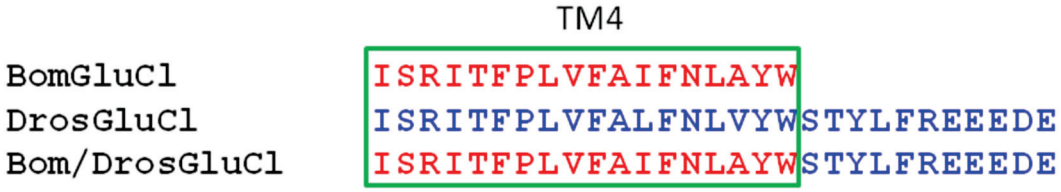

Fig. 4. C-terminal amino acid sequences of *Bombyx* GluCl (accession No. AB857001), *Drosophila* GluCl-α (accession No. U58776), and the chimera (*Bombyx*/*D*-GluCl).

[^{3}H]IVM B_{1a} competition assays

Competition assays were performed as previously described (Yamaguchi et al., 2012). After transfection, the cells were washed twice with 800 µl of 1×Dulbecco's phosphate buffered saline (Life Technologies). The cells were homogenized in 50 mM HEPES buffer (pH 7.4) using a Teflon-glass homogenizer, and the homogenates were centrifuged at 25,000×*g* for 30 min at 4 °C. The pellet was suspended in 50 mM 4-(2-hydroxyethyl)-1-piperazineethanesulfonic acid (HEPES) buffer (pH 7.4). The amount of protein was determined by the Bradford method using bovine serum albumin

as the standard (Bradford, 1976).

Cell membranes (protein, 20 μg) were incubated with 1 nM (in *Bombyx*/*D*-GluCls) or 0.5 nM (in Hco-AVR-14B-GluCls) [^{3}H]IVM B_{1a} in 500 μl of 50 mM HEPES buffer (pH 7.4) containing 0.02% (v/v) Triton X-100 for 1 h at 37 °C. Nonspecific binding was determined in the presence of 1 μM unlabeled IVM B_{1a}. Ligand competition was determined using 100 pM-10 μM PPs. After the incubation, the mixtures were filtered through Whatman GF/B filters treated with 50 mM HEPES buffer containing 0.1% polyethyleneimine using a Brandel M-24 cell harvester. Cell membranes on the filters were washed twice with 5 ml of distilled water containing 0.25% (v/v) Triton X-100. Radioactivity on the filters was measured using a liquid scintillation counter. Each experiment was performed in triplicate and repeated three times. Fifty-percent inhibitory concentrations (IC_{50}s) were determined from concentration-inhibition curves using OriginPro 8 SR4 (v8.0951). The inhibition constants (K_is) of PPs were calculated from IC_{50}s according to Cheng and Prusoff (Cheng and Prusoff, 1973); in the calculation, the dissociation constants (K_ds) of IVM B_{1a}, 0.35 nM (McCavera et al., 2009) and 0.41 nM, were used for Hco-AVR-14B-GluCls and *Bombyx*/*D*-GluCls, respectively. The K_d of [^{3}H]IVM B_{1a} in *Bombyx*/*D*-GluCls was obtained from the slope of linear Scatchard plots (Scatchard, 1949); 0.075-9.6 nM [^{3}H]IVM B_{1a} was used in this experiment.

Determination of the ability of PPs to activate GluCls

Expression of Hco-AVR-14B-GluCls in Xenopus oocytes

Oocyte isolation, cRNA synthesis, and protein expression were performed as previously described (Kita et al., 2014). Briefly, the lobes of the ovary were pull out surgically from female African clawed frogs (*Xenopus laevis*) anesthetized by immersion in a 0.1% (w/v) 3-aminobenzoic acid ethyl ester methanesulfonate (tricaine) solution. Follicle cells were treated with collagenase (2 mg/ml; Sigma-Aldrich) in a calcium-free standard oocyte solution (Ca^{2+} free SOS) (100 mM NaCl, 2 mM KCl, 1 mM $MgCl_2$, 5 mM HEPES, pH 7.6) for 1-2 h at 20 °C. After the treatment, the oocytes were washed with SOS (100 mM NaCl, 2 mM KCl, 1.8 mM $CaCl_2$, 1 mM $MgCl_2$, 5 mM HEPES, pH 7.6) supplemented with 2.5 mM sodium pyruvate, gentamycin (50 μg/ml; Thermo Fisher Scientific, Waltham, MA), penicillin (100 U/ml; Thermo Fisher Scientific), and streptomycin (100 μg/ml; Thermo Fisher Scientific) and incubated for 1-2 day at 16 °C.

The cDNA template containing a T7 RNA polymerase promoter site upstream of the Hco-AVR-14B coding region was PCR amplified from pcDNA3-Hco-AVR-14B using KOD -Plus- Ver. 2 (Toyobo) and in vitro transcribed into capped cRNA using T7 polymerase in mMESSAGE mMACHINE® T7 Ultra Kit (Life Technologies) and the template (100 ng). Transcribed cRNAs were evaluated for quality and quantity by agarose gel electrophoresis and absorption spectroscopy, respectively. cRNA (5 ng in 9.2 nl of nuclease-free water) was injected into each oocyte using a Nanoliter 2000 injector (World Precision Instruments, Sarasota, FL). The injected oocytes were incubated for 2-3 days at 16 °C prior to recording.

Two-electrode voltage clamp electrophysiology (TEVC)

TEVC assays were performed as previously described (Kita et al., 2014). Oocytes microinjected with cRNA were immobilized in a chamber, which was then perfused with standard oocyte solution (SOS). The glass micro-electrodes were filled with 2 M KCl with a resistance of 0.5-1.6 MΩ. Membrane currents were recorded using an Oocyte Clamp OC-726C amplifier (Warner Instruments, Hamden, CT) at a holding potential of -80 mV. Data were digitized using a Lab-Trax-4/16 converter (World Precision Instruments) and analyzed using Data-Trax2 software (World Precision Instruments). Experiments were performed at 20 °C. Each experiment was replicated using at least six oocytes from at least two frogs. Glu was dissolved in SOS at 300 μM and applied to oocytes for 3 s. IVM B_{1a} and PPs dissolved in dimethyl sulfoxide (DMSO) were diluted with SOS (DMSO, 0.01%) and applied to oocytes for 30 s. After each treatment with IVM, oocytes were washed by SOS for more than 20 min.

Solubilization of GluCl protein expressed in COS-1 cells and Xenopus oocytes

The Hco-AVR-14B-GluCls were expressed in COS-1 cells and *Xenopus* oocytes. The membrane proteins from COS-1 cells were prepared as previously described (Yamaguchi et al., 2012; Chapter 2, *[^{3}H]IVM B_{1a} competition assays*). Fifty oocytes were chosen from oocytes that responded to 300 μM Glu with induced currents of > 400 nA and homogenized in 50 mM HEPES buffer (pH 7.4) using a Teflon-glass homogenizer, and the homogenates were centrifuged at 500×*g* for 5 min at 4 °C. The supernatants were centrifuged at 25,000×*g* for 30 min. The supernatants were removed, and the pellets were suspended in 50 mM HEPES buffer and centrifuged at 25,000×*g* for 30 min. The pellet was washed four times to remove yolk granules. The COS-1 cell

membranes and oocytes pellets were separately resuspended in 50 mM HEPES buffer and 0.05% (w/v) *n*-dodecyl-β-D-maltopyranoside (DDM) solution. These mixtures were incubated for 1 h at 4 °C, and centrifuged at 125,000×*g* for 1 h at 4 °C. The supernatants were used for the photoaffinity labeling.

[^{3}H]IVM B_{1a} competition assays using solubilized proteins

Solubilized COS-1 cells or oocyte proteins (200 μg) were incubated with 1 nM [^{3}H]IVM B_{1a} in 500 μl of 50 mM HEPES buffer (pH 7.4) containing 0.02% (v/v) Triton X-100 for 1 h at 37 °C. Nonspecific binding was determined in the presence of 1 μM unlabeled IVM B_{1a}. After the incubation, 20% (w/v) polyethylene glycol 6000 solution (final concentration, 10%) was added to the mixture, and the mixture was incubated for 15 min at 37 °C. The mixtures were filtered through Whatman GF/B filters treated with 50 mM HEPES buffer containing 0.1% polyethyleneimine using a Brandel M-24 cell harvester. Cell membranes on the filters were washed twice with 5 ml of distilled water containing 0.25% (v/v) Triton X-100. Radioactivity on the filters was measured using a liquid scintillation counter.

Photoaffinity labeling experiments

Solubilized oocyte membrane protein (200 μg) and **[^{125}I]IodoPP2** (2 μM) were incubated for 1 h at 22 °C. Nonspecific binding was determined in the presence of 10 μM unlabeled IVM B_{1a}. After the incubation, the mixture was irradiated with a long wavelength ultraviolet (UV) lamp (Black-lay model B-100A, UVP, Upland, CA) for 1 h on ice, placed 10 cm from the light source. After the irradiation, a 4-fold volume of MeOH was added to the mixture, which was then incubated at -20 °C for 1 h. The pellets were centrifuged at 14000 rpm for 10 min at 4 °C, and the supernatants were removed.

The reaction mixture was suspended in Laemmli buffer and boiled for 3 min at 96 °C. The lysate was loaded onto a 10% sodium dodecyl sulfate (SDS)-polyacrylamide gel with a 5% stacking gel. Then, the gel was stained with Coomassie brilliant blue R-250, dried for 1 h at 80 °C, exposed to an imaging plate, and visualized with a (BAS-1500, Fuji Film). After visualizing, the gel was cut into 2-mm strips, and the radioactivity in each strip was measured by γ-counting system (COBRA II5003, PerkinElmer).

Results

Synthesis of PPs

In the present study, three IVM B_{1a} derivatives were synthesized. In three derivatives, the bisoleandrosyl group at C-13 was replaced with a photoreactive 4'-(4-azidobenzoyl)oleandrosyl (**PP1**), 3-(4-azidobenzamido)propionyl (**PP2**) or 3-(6-(4-azidobenzamido)hexanamide)propionyl group (**PP3**). These compounds were characterized by their ^{1}H NMR and HRMS.

To synthesize **PP1**, monosaccharide **1** was prepared by the methanolysis of IVM B_{1a} with 1% sulfuric acid in MeOH (Scheme 1). Selective silylation of the 5-hydroxy group of **1** with TBDMSCl resulted in 5-*O*-TBDMS ether **2**. Ester **3** was prepared by reacting 4-azidobenzoic anhydride, prepared from 4-azidobenzoic acid in the presence of triethylamine, with **2** in the presence of DIPEA and DMAP in quantitative yield. Desilylation of the 5-*O*-TBDMS group of **3** with HF-pyridine (7:3) yielded **PP1**.

Methanolysis of IVM B_{1a} with 10% sulfuric acid in MeOH yielded aglycone **4**, the 4-hydroxyl group of which was then silylated to generate **5** (Scheme 2). Ester **6** was prepared from **5** and *N*-Troc-β-alanine in a manner similar to the synthesis of **3**. The Troc group was then removed by reduction with zinc powder to yield **7**. After acylation of the amino group of **7** with 4-azidobenzoic acid in the presence of DCC to produce benzamide **8**, **PP2** was obtained by desilylation of the *O*-TBDMS group of **8** with HF-pyridine (7:3).

To synthesize **PP3**, amide **9** was generated from the acylation of the amino group of **7** with *N*-Troc-6-aminohexanoic acid in the presence of EDC and HOBt (Scheme 3). The Troc group was then removed using zinc powder in the presence of AcOH/H_2O (10:1) to yield **10**. After the reaction of **10** with 4-azidobenzoic acid in the presence of EDC and HOBt, **PP3** was obtained by desilylation of the *O*-TBDMS group of **11** using HF-pyridine (7:3).

*Affinity of **PP1**−**3** for GluCls*

To examine whether **PP1**, **2**, and **3** interact with GluCls with high affinity, competition assays using the radioligand [^{3}H]IVM B_{1a} were perfomed. Two types of GluCls cloned from the parasitic nematode *Haemonchus contortus* and the silkworm *Bombyx mori* were used. Hco-AVR-14B-GluCls was previously shown to be activated by binding IVM B_{1a} and MLM A_4 (Cheeseman et al., 2001; Forrester et al., 2002;

McCavera et al., 2009; Yanaguchi et al., 2012). These GluCls were transiently expressed as homomeric channels in COS-1 cells. The IC_{50}s of **PP1**−**3** inhibiting specific [^{3}H]IVM B_{1a} binding to the membranes of COS-1 cells expressing GluCls were determined. The concentration-inhibition curves are shown in Fig. 5. The K_i values derived from IC_{50}s are presented in Table 1. Synthesized PPs inhibited [^{3}H]IVM B_{1a} binding with low- or subnanomolar K_is in Hco-AVR-14B-GluCls; the potencies of **PP1**, **2**, and **3** in these channels were 2-, 27- and 16-fold higher than those in *Bombyx*/*D*-GluCls, respectively. Overall, our data show that **PP2** has high affinity for Hco-AVR-14B-GluCls, followed by **PP3**.

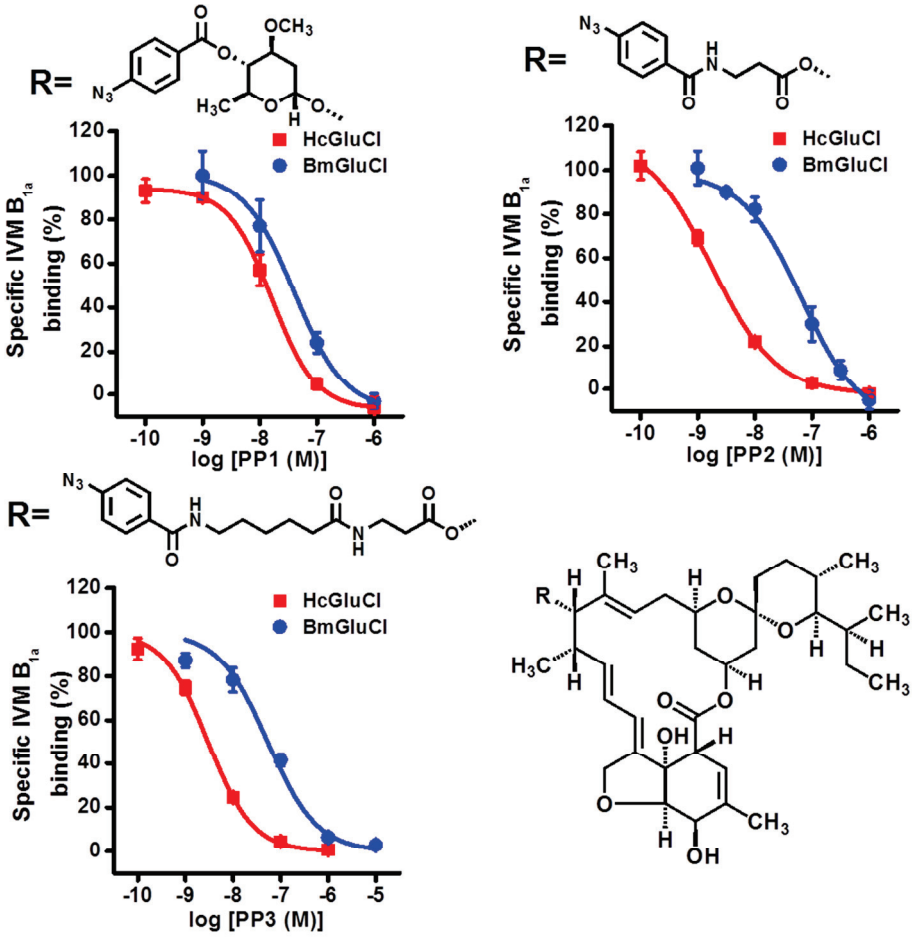

Fig. 5. Inhibition of [^{3}H]IVM B_{1a} binding to the membranes of COS-1 cells transiently expressing Hc (red squares)- and *Bombyx/D* (blue circles)-GluCls. The ability of three PPs to inhibit specific [^{3}H]IVM B_{1a} binding to the membranes was determined at various concentrations. Error bars denote standard error of the mean (SEM) (n=3).

Table 1. Potencies (K_is) of PPs in inhibiting [^{3}H]IVM B_{1a} binding to GluCls expressed in COS-1 cells

PP	K_i (nM)	
	Hco-AVR-14B-GluCl	*Bombyx*/*D*-GluCl
1	7.94 ± 2.60	12.1 ± 2.0
2	0.874 ± 0.277	23.4 ± 4.8
3	1.48 ± 0.31	23.2 ± 3.8

Data are the means ± SEM (n = 3).

*Activation of Hco-AVR-14B-GluCls by **PP1−3***

Next, it was examined whether **PP1**, **2**, and **3** possess the ability to activate Hco-AVR-14B-GluCls expressed in *Xenopus* oocytes using a TEVC technique. Application of 300 μM Glu to oocytes injected with Hco-AVR-14B-GluCls subunit cRNA induced rapidly activating reversible currents, whereas application of 100 nM IVM induced slow long-lasting currents (Fig. 6A). The IVM-induced currents are comparable to those reported to date (Cully et al., 1994). **PP1** induced slowly and irreversibly activated currents at 300 nM but not at 100 nM (Fig. 6B). **PP2** activated similar currents at 30 and 100 nM (Fig. 6C). Although the application of 30 nM **PP3** activated minimal currents, it evoked robust currents at 100 nM (Fig. 6D). The maximal currents elicited with IVM B_{1a}, **PP2**, and **PP3** were 9.5 ± 3.0%, 20.8 ± 1.3%, and 14.2 ± 3.3%, respectively, of the maximal currents elicited by Glu when compared at 100 nM (Fig. 6E). These findings indicate that, of the three probes, **PP2** is potent and efficacious in functional assays using Hco-AVR-14B-GluCls.

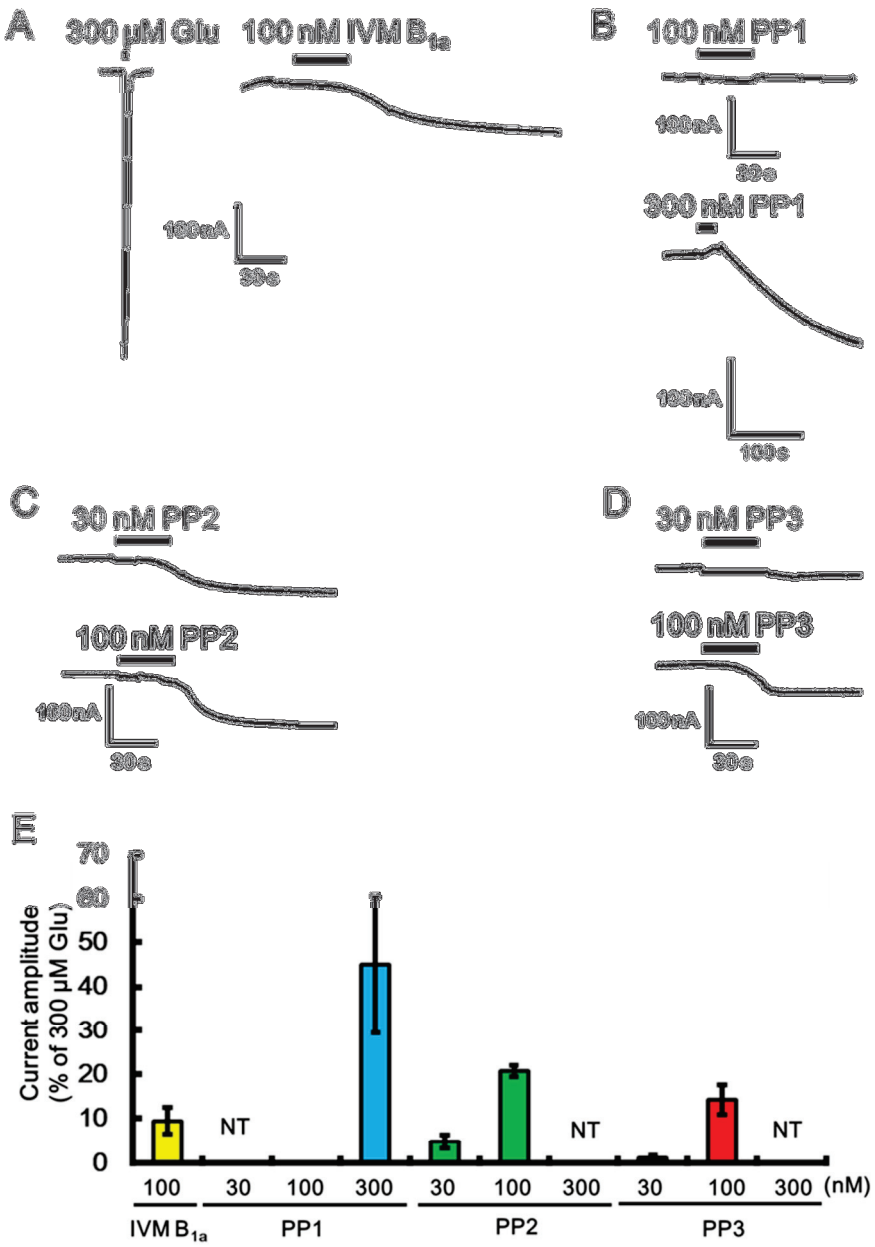

Fig. 6. Activation of Hco-AVR-14B-GluCls expressed in *Xenopus* oocytes. (A) Traces of currents induced by Glu and IVM B_{1a}. (B) Traces of currents induced by **PP1**. (C) Traces of currents induced by **PP2**. (D) Traces of currents induced by **PP3**. (E) Current amplitudes induced by PPs relative to 300 µM Glu. NT, not tested. Error bars denote SEM (n=6-13).

*Synthesis and affinity of **IodoPP2***

To prepare **[^{125}I]IodoPP2**, 13-*O*-[3-(2-hydroxyl-4-azido-5-iodobenzoylamino)-

propanoyl]IVM B_{1a} (**IodoPP2**) was synthesized because **PP2** was the most potent and efficacious for Hco-AVR-14B-GluCls (Scheme 4). First, 2-hydroxyl-4-azido-5-iodo-benzoic acid (**15**) was synthesized from 2-hydroxyl-4-aminobenzoic acid in four steps. This compound was converted to succinate imide (**16**) with *N*-hydroxysuccinimide and EDC, and **17** was synthesized by the reaction of **7** with **16** with stirring at room temperature for 72 h. **IodoPP2** was obtained by desilylation of the *O*-TBDMS group of **17** with HF-pyridine (7:3).

To examine whether **IodoPP2** interacts with Hco-AVR-14B-GluCls with high affinity, competition assays were conducted using the radioligand [^{3}H]IVM B_{1a} as the affinity measurements of **PP2**. **IodoPP2** inhibited [^{3}H]IVM B_{1a} binding with an IC_{50} of 1.15 ± 0.29 nM, and the potencies of **IodoPP2** and **PP2** did not greatly differ (Fig. 7).

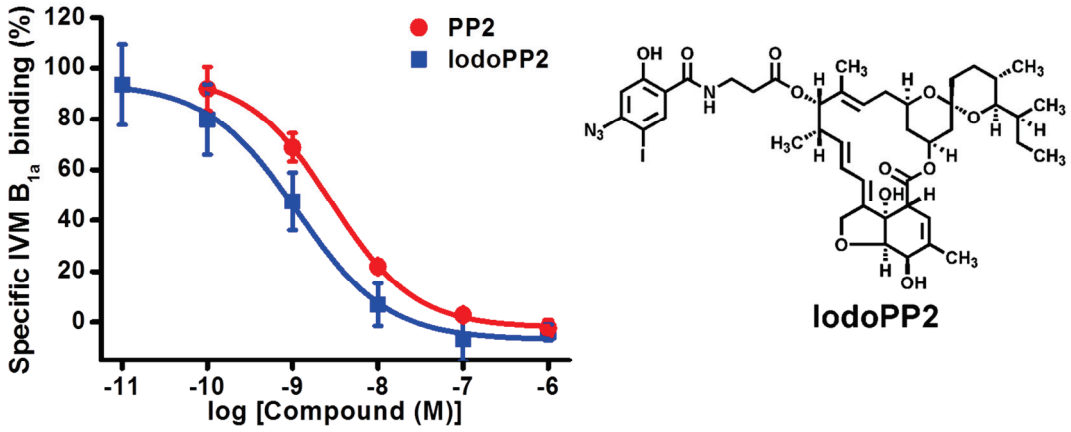

Fig. 7. Inhibition of [^{3}H]IVM B_{1a} binding to the membranes of COS-1 cells transiently expressing Hco-AVR-14B-GluCls. The ability of **PP2** (red, circles) and **IodoPP2** (blue, squares) to inhibit specific [^{3}H]IVM B_{1a} binding to the membranes was determined at various concentrations. Error bars denote SEM (n=3).

Synthesis of radiolabeled ***[^{125}I]IodoPP2***

Chloramine-T is commonly used in radiolabeling of small molecules and proteins by iodination. **[^{125}I]IodoPP2** was synthesized by the replacement of the iodine group of **IodoPP2** with [^{125}I]NaI in the presence of chloramine-T (Scheme 5). The radiolabeled probe with a specific activity of 1.2 Ci/mmol was obtained in a pure form by preparative TLC.

Binding of [^{3}H]IVM B_{1a} to proteins solubilized from COS-1 cell and oocyte membranes

COS-1 cell and oocyte membranes were solubilized by 0.05% DDM solution. Specific [^{3}H]IVM B_{1a} binding levels were assessed in solubilized proteins from COS-1 cell and oocyte membranes. The amount of [^{3}H]IVM B_{1a} bound to proteins solubilized from oocyte membranes was approximately 70-fold greater than those from COS-1 cell membranes (Fig. 8). Therefore, proteins solubilized from oocyte membranes were used to examine the photoaffinity labeling using **[^{125}I]IodoPP2**.

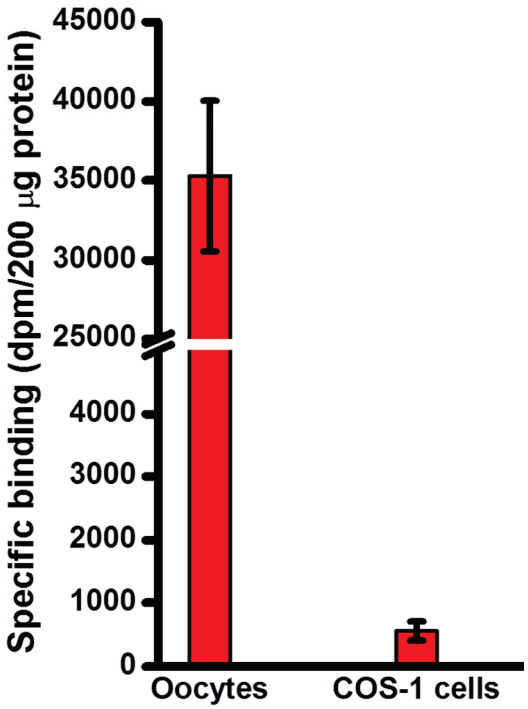

Fig. 8. Specific binding of [^{3}H]IVM B_{1a} to proteins solubilized from *Xenopus* oocyte and COS-1 cell membranes. The data are the means ± SEM of three experiments.

Photoaffinity labeling of Hco-AVR-14B-GluCls by ***[^{125}I]IodoPP2***

The photolabeled protein was visualized by autoradiography after SDS-PAGE, and the gel, which was cut into 2-mm strips, was measured for radioactivity by γ-counting system (Fig. 9). In the SDS gel, no band of specifically photolabeled Hco-AVR-14B-GluCls (50 kDa) was detected. UV irradiation of solubilized proteins in the presence of **[^{125}I]IodoPP2** did not result in photo-cross linked bands on the SDS gel.

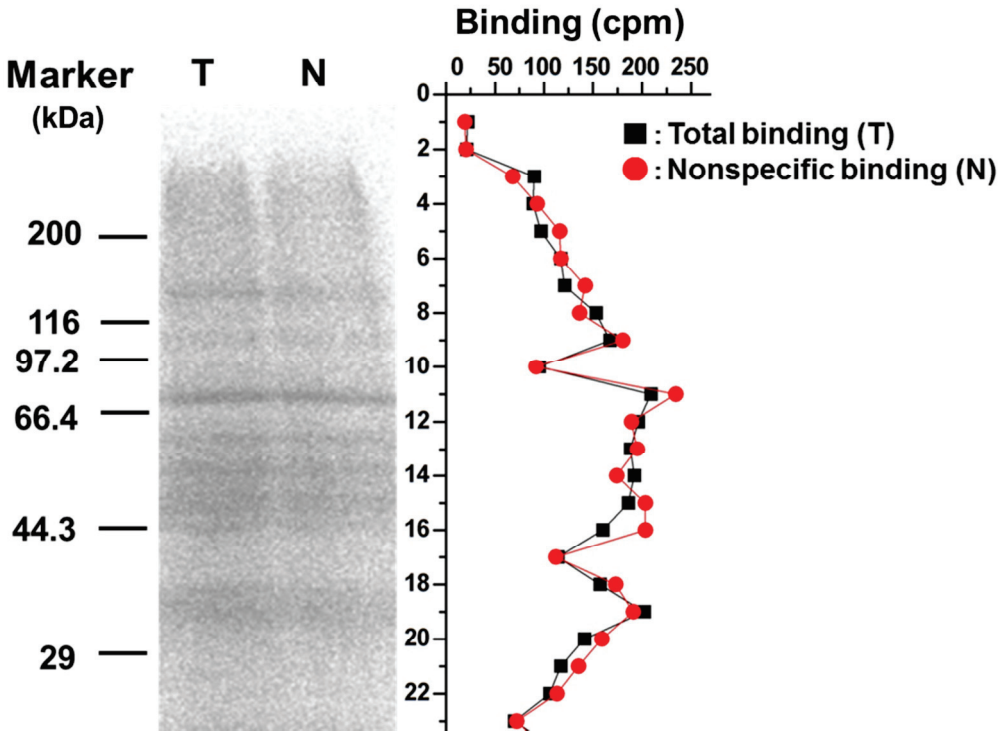

Fig. 9. The results of photoaffinity labeling experiments using solubilized protein from *Xenopus* oocytes expressing Hco-AVR-14B-GluCls with [^{125}I]IodoPP2. The SDS-PAGE bands were visualized by autoradiography (left). T, total binding; N, nonspecific binding. The gel was cut into 2 mm strips and the radioactivity was measured by γ-counting system (right).

Discussion

The macrocyclic anthelmintics/insecticides AVMs and IVM act at ligand-gated ion channels that are activated by Glu, GABA, glycine, acetylcholine, and ATP (Zemkova et al., 2014). Earlier extensive studies indicated the macrolide potentiation, activation, and antagonism of invertebrate and vertebrate GABACls (Huang and Casida, 1997; Duce and Scott, 1985; Dawson et al., 2000). Since the encoding cDNAs were cloned (Cully et al., 1994 and 1996), GluCls have been highlighted as a primary target; the expression studies showed that the macrolides potentiate or activate GluCls. However, it remains to be investigated to what extent the interaction with each type of the channels contributes to the insecticidal, acaricidal, or nematicidal activities of the macrolides.

Previously, several photoreactive AVM analogs were synthesized to identify AVM-binding proteins (Meinke et al., 1992; Tsukamoto et al., 2000). Of these analogs, AVM B_{1a} with 3-(6-(4-azido-3-^{125}iodo-2-hydroxylbenzamido)hexanamide)propanamido

group at C-4'' of the bisoleandrosyl moiety ([^{125}I]azido-AVM) was reported to label ≈12, ≈47, ≈53 kDa proteins from *C. elegans* and ≈45 or ≈47 kDa protein from *D. melanogaster*, and 45 kDa protein from the American grasshopper *Schistocerca americana* (Rohrer et al., 1992 and 1995). In addition, ≈45 and ≈50 kDa proteins were over 9000-fold purified using immunoaffinity chromatography (Rohrer et al., 1994). Ester-type and ether-type PPs of AVM B_{1a} were synthesized and examined for their abilities to inhibit the binding of [^{3}H]AVM B_{1a} to membranes prepared from mouse brain, housefly and fruit fly heads (Tsukamoto et al., 2000). These PPs showed low- to mid-nanomolar IC_{50}s, but the results of photoaffinity labeling were not reported.

The above-mentioned photoaffinity labeling studies were performed before the GluCl genes were cloned. In the present study, three photoreactive IVM B_{1a} analogs, **PP1**−**3**, were synthesized. These three PPs bind to GluCls with low-nanomolar affinity and were able to activate GluCls. Of the three PPs, **PP2** was superior in both affinity and function at Hco-AVR-14B-GluCls.

[^{125}I]IodoPP2 was used to photolabel Hco-AVR-14B-GluCls solubilized from oocyte membranes. However, no specific cross-linked band with Hco-AVR-14B-GluCls was detected in the SDS gel. X-ray crystallographic analysis indicated that the dioleandrosyl group of IVM is located outside of the *C. elegans* GluCl when IVM was co-crystalized with the GluCl (Hibbs and Gouaux, 2011). The azido group of **[^{125}I]IodoPP2** could be located at the same position of the dioleandrosyl group of IVM B_{1a}. This could be the reason why the azido group of **IodoPP2** was not capable of covalently reacting with Hco-AVR-14B-GluCls. These results suggest that a photoreactive functional group should be introduced into a position near the macrocyclic lactone ring of IVM in the future study.

Chapter 3

Electrophysiological characterization of IVM triple actions on *Musca* GABACl and GluCl

Introduction

IVM was reported to modulate various ion channels such as $GABA_A$Rs, nAChRs, $P2X_4$Rs, and GlyRs in vertebrates (Adelsberger et al., 2000; Khakh et al., 1999; Krause et al., 1998; Krůšek and Zemková, 1994; Shan et al., 2001; Sigel and Baur, 1987). IVM 4''-*O*-phosphate ($IVMPO_4$), a water-soluble IVM analog, was reported to act at *C. elegans* GluCls to elicit currents by itself (activation) at high nanomolar concentrations and to enhance Glu-induced currents (potentiation) at low nanomolar concentrations (Cully et al., 1994). $IVMPO_4$ activated currents in *Drosophila* GluCls, whereas it only slightly potentiated Glu-induced currents (Cully et al., 1996). Aside from the actions on GluCls, IVM was recently shown to act on *Drosophila* GABACls as an allosteric agonist or an antagonist (Lees et al., 2014; Nakao et al., 2015).

This chapter describes the results of electrophysiological analyses performed to clarify what type of action of IVM on insect GluCls or GABACls plays major roles in the manifestation of their insecticidal effects. The results indicated that IVM has a unique triple action (activation, potentiation, and antagonism) on both GluCls and GABACls cloned from houseflies (*Musca domestica*), depending on application conditions. In all these actions, GluCls were more sensitive to IVM than GABACls.

Material and methods

Chemicals

GABA, sodium hydrogen Glu, and general chemicals were purchased from Wako Pure Chemical Industries, Ltd. (Osaka, Japan), unless otherwise noted. IVM was the same as IVM used in Chapter 2.

Insecticidal assays of IVM on houseflies

IVM solutions of five different concentrations (1-10 ng/μl) in acetone were prepared. One μl of each solution was topically applied on the dorsal surface of 30 CO_2-anesthetized adult female houseflies (WHO/SRS strain) using an Arnold hand microapplicator (Burkard, Scientific Ltd., Rickmansworth, UK). The flies were maintained with sugar and water at 25 °C. Mortality was assessed 24 h after the treatment. This assay was replicated three times.

Introduction of mutations into cDNAs encoding Musca GluCl and GABACl subunits

cDNAs, *GluCl* and *Rdl*, that encode *Musca* GluCl (variant A) and GABACl (Rdl variant ac) subunits, respectively, were subcloned into the pBluescript KS(-) vector in our previous studies (Eguchi et al., 2006; Ozoe et al., 2013). Introduction of mutations into *GluCl* and *Rdl* was performed using QuikChange Site-Directed Mutagenesis Kit (Agilent Technologies, Santa Clara, CA) and verified by DNA sequencing.

Preparation of cRNA and injection into oocytes

Preparation of cRNA was performed as Chapter 2. The *Musca GluCl* and the *Rdl* cDNAs containing a T7 promoter site upstream of the coding region were amplified by PCR using the primers M13 and M13 Reverse. The PCR products were purified using illustra GFX PCR DNA and Gel Band Preparation Kit (GE Healthcare Bio-Sciences, Pittsburgh, PA). After sequence verification, the amplified cDNA templates (100 ng) were *in vitro* transcribed into capped poly(A) cRNAs using mMESSAGE mMACHINE® T7 Ultra Kit (Thermo Fisher Scientific). The quality and the quantity of the prepared cRNAs were evaluated by agarose gel electrophoresis and absorption spectroscopy, respectively. Purified cRNA (25-30 ng in 46.0-55.2 nl of nuclease-free water) was injected into each oocyte using a Nanoliter 2000 injector (World Precision Instruments, Sarasota, FL). Oocytes isolation was performed as Capter 2. The injected oocytes were incubated for 1-2 days at 16 °C prior to electrophysiological experiments.

Two-electrode voltage clamp electrophysiology

The oocytes expressing *Musca* GluCls or GABACls were immobilized in a chamber perfused with SOS. The glass micro-electrodes were filled with 2 M KCl to

yield the resistance of 0.5-1.6 MΩ. Electrophysiological recordings were made using an Oocyte Clamp OC-726C amplifier (Warner Instruments, Hamden, CT) at a holding potential of -80 mV at 20 °C. Data were digitized using a Lab-Trax-4/16 converter (World Precision Instruments) and analyzed using Data-Trax2 software (World Precision Instruments). Glu and GABA was dissolved in SOS and applied to oocytes for 3 s. IVM dissolved in DMSO was diluted with SOS to produce perfusates containing given concentrations of IVM and less than 0.01% DMSO. Oocytes were perfused with the IVM solution for 3 min to analyze channel activation by IVM. In the analysis of potentiation and inhibition by IVM, Glu or GABA was applied for 3 s at 30 s intervals with the perfusion of IVM. Each experiment was replicated using at least six oocytes from at least two frogs. The data are presented as means ± SEM. Statistical significance was evaluated using unpaired *t*-test.

Homology modeling

The amino acid sequences of the *M. domestica* GluCl A subunit and the *C. elegans* GluCl α subunit were aligned using ClustalW2. A *Musca* GluCl homology model was constructed using MOE software (version 2014.04; Chemical Computing Group, Montreal, Canada). The X-ray crystal structure of the *C. elegans* GluCl-α channel (PDB code: 3RHW) was used as a template.

Results

Insecticidal effects of IVM on houseflies

The insecticidal activity of IVM against adult female houseflies was first examined. IVM did not cause convulsion but immobilized flies, followed by death with an LD_{50} of 3.8 ± 0.15 ng/fly.

Responses of GluCls and GABACls to agonists

It was examined whether *Musca* GluCls and GABACls expressed in *Xenopus* oocytes are responsive to Glu and GABA, respectively. The channels tested included wild-type GluCls, G36'M GluCls, wild-type GABACls, G36'M GABACls, and G36'A GABACls. All channels including mutants showed robust responses to agonists, generating rapid inward currents. The agonist concentration-response curves gave half

maximal effective concentrations (EC_{50}s) of 7.85 and 299 μM for wild-type and G36'M GluCls, respectively (Fig. 10A, Table 2), and EC_{50}s of 17.9, 115, and 86.5 μM for wild-type, G36'M, and G36'A GABACls, respectively (Fig. 10B, Table 2). G36'M GluCls showed lower sensitivity to Glu than wild-type GluCls ($p < 0.01$). The EC_{50}s of G36'M and G333A GABACls were not significantly different, but both mutants were less sensitive to GABA than wild-type GABACls ($p < 0.01$).

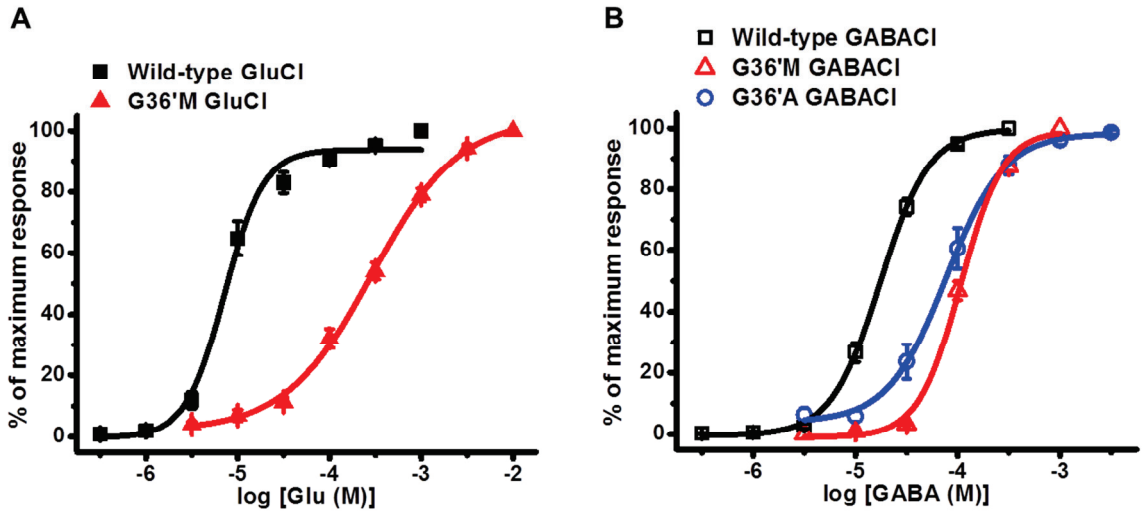

Fig. 10. Agonist activation of *Musca* GluCls and GABACls expressed in *Xenopus* oocytes. (A) Glu concentration-response curves in wild-type and G36'M GluCls. Error bars indicate SEM (n=6). (B) GABA concentration-response curves in wild-type, G36'M, and G36'A GABACls. Error bars indicate SEM (n=6-8).

Table 2. Agonist (Glu and GABA) profiles in *Musca* GluCls and GABACls

Channel		EC_{50} (μM)	n_H[a]
GluCl	Wild-type	7.85 ± 1.20	2.09 ± 0.19
	G312M	299 ± 32	0.940 ± 0.046
GABACl	Wild-type	17.9 ± 1.6	1.89 ± 0.09
	G333M	115 ± 9	2.21 ± 0.11
	G333A	86.5 ± 15.3	1.87 ± 0.22

[a]Hill coefficient. Data are the means of 6-8 experiments ± SEM.

Actions of IVM on GABACls

IVM alone elicited slow, sustained currents when perfused on oocytes expressing wild-type GABACls for 3 min (Fig. 11A), with an EC_{50} of 1.25 ± 0.40 μM, which is

184-fold larger than the EC_{50} of IVM in wild-type GluCls ($p < 0.05$) (Table 3). G36'M GABACls showed no response to IVM (Fig. 11B and C). G36'A GABACls responded to IVM, with smaller amplitudes of currents compared to those of wild-type GABACls (Fig. 11B).

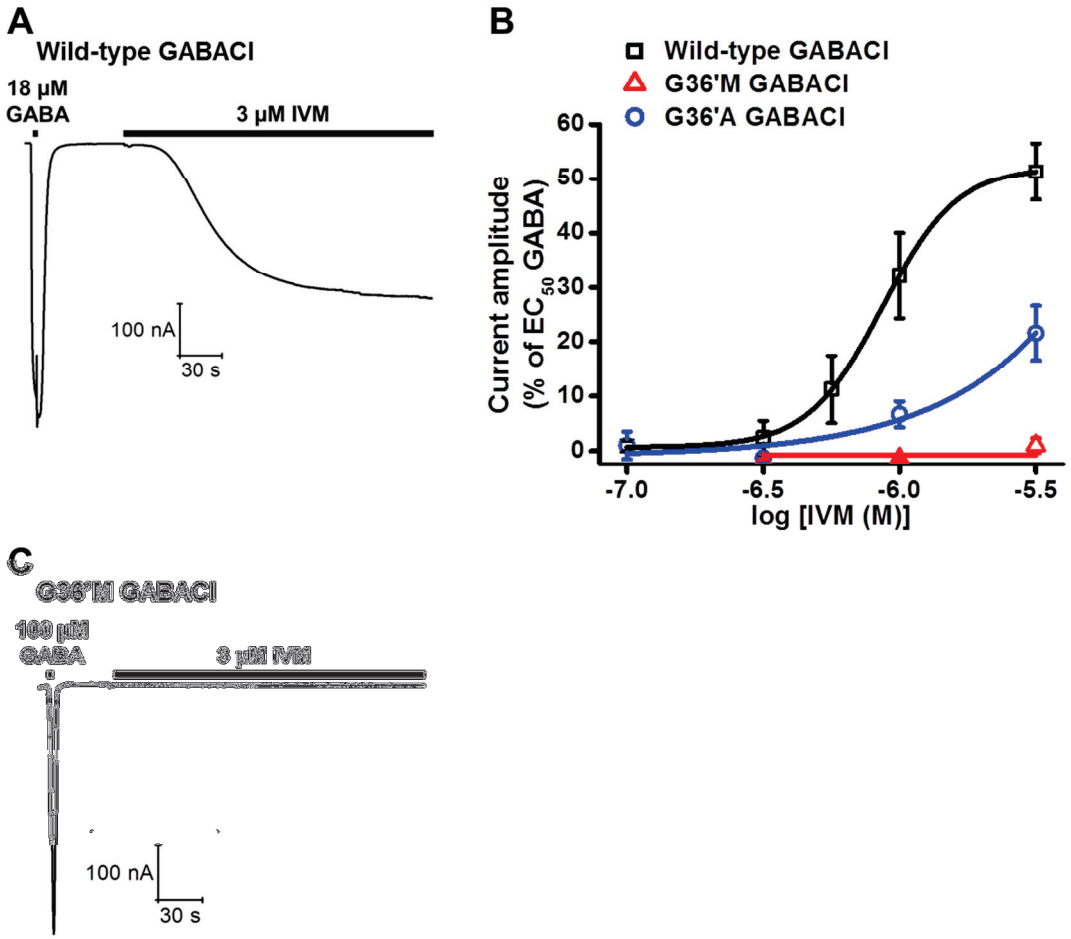

Fig. 11. IVM activation of wild-type, G36'M, and G36'A GABACls. (A) A trace of a current induced by IVM administered to wild-type GABACls. (B) IVM concentration-response curves in the activation in wild-type, G36'M, and G36'A GABACls. Error bars indicate SEM (n=6). (C) A current trace when IVM was administered to G36'M GABACls.

When GABA was applied to oocytes expressing wild-type GABACls, the amplitude of currents induced by GABA below 18 μM (EC_{50}) was increased by the perfusion of 1-300 nM IVM (Fig. 12). Currents induced by 1 μM (EC_5) GABA were potentiated by 30 nM IVM (Fig. 13A). We examined the concentration-dependence of IVM potentiation induced by 1 μM (EC_5) GABA in wild-type GABACls. The

potentiation was concentration-dependent with a maximum at 100 nM IVM and decreased with >300 nM IVM in wild-type GABACls (Fig. 13B). The EC_{50} of IVM was estimated to be 46.7 ± 1.9 nM, with maximal potentiation at 100 nM. EC_5 (20 μM) GABA-induced currents were little potentiated by IVM in G36'M GABACls (Fig. 13B and C). Although the potentiation of EC_5 (10 μM) GABA-induced currents were most efficacious (approximately 230-fold relative to the amplitude of currents induced by EC_5 GABA alone) in G36'A GABACls, the potency of IVM was approximately 6-fold reduced compared with wild-type GABACls; the EC_{50} being 294 ± 47 nM (Fig. 13B and D).

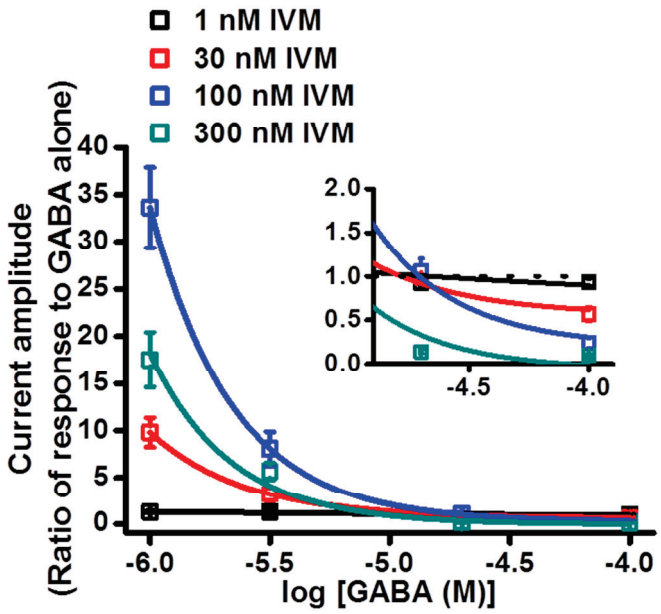

Fig. 12. IVM potentiation and inhibition of wild-type GABACls. Concentration-response curves for the IVM potentiation and inhibition of currents induced by different concentration of GABA in wild-type GABACls. Inset shows the expansion of the concentration-response curves in the range of high GABA concentrations. Error bars indicate SEM (n=6-15).

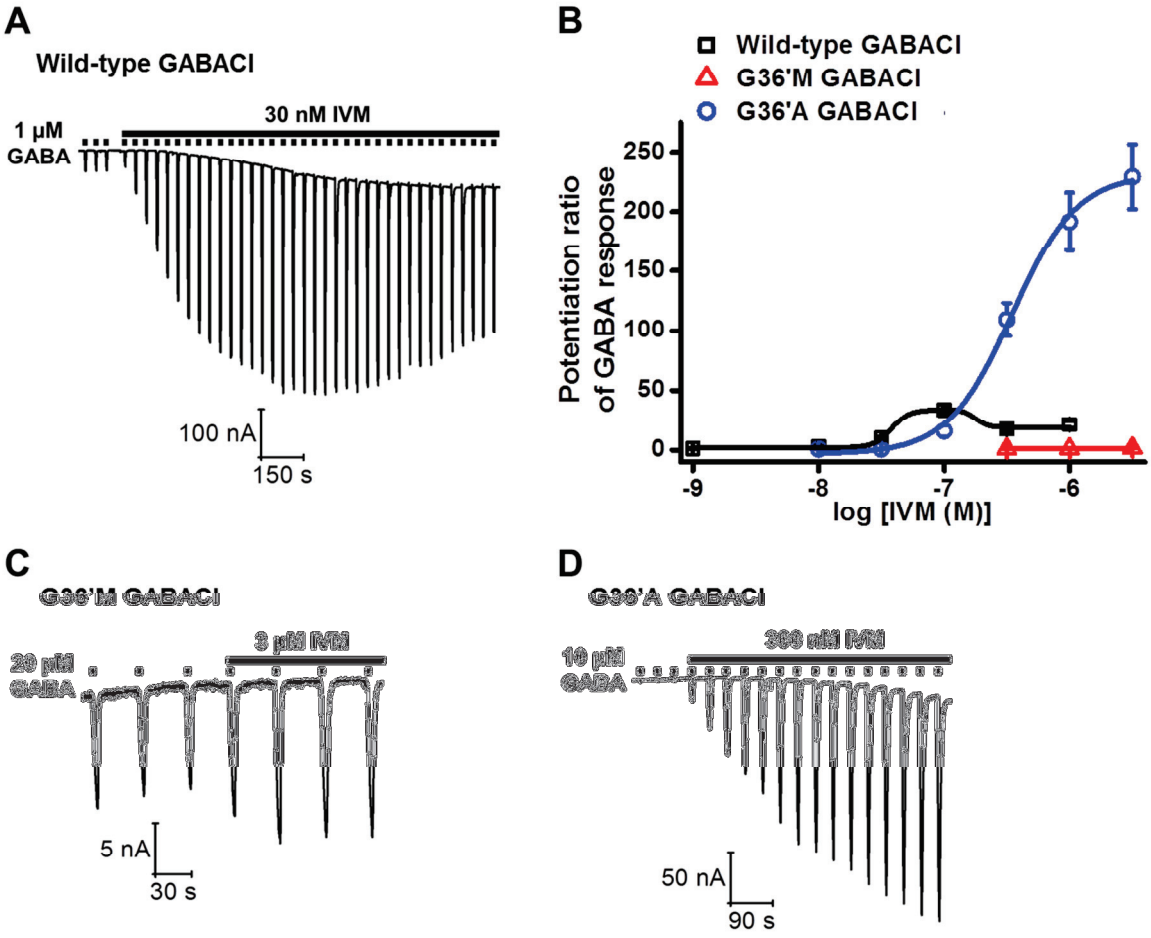

Fig. 13. IVM potentiation of currents induced by EC_5 GABA in wild-type, G36'M, and G36'A GABACls. (A) A current trace showing the IVM potentiation of currents in wild-type GABACls. (B) IVM concentration-response curves for the potentiation of GABA-induced currents in wild-type, G36'M, G36'A GABACls. Error bars indicate SEM (n=6-15). (C) A current trace showing the IVM potentiation of currents in G36'M GABACls. (D) A current trace showing the IVM potentiation of currents in G36'A GABACls.

When GABA above 18 μM (EC_{50}) was applied to oocytes expressing wild-type GABACls with the perfusion of IVM, currents elicited by GABA were reduced by IVM (Fig. 12). When 100 μM (EC_{90}) GABA was applied with the perfusion of IVM, GABA-induced currents were inhibited by 300 nM IVM in wild-type GABACls (Fig. 14A). The IC_{50} of IVM for wild-type GABACls was 42.0 ± 7.7 nM. Currents induced by the EC_{90} (500 μM) of GABA were not inhibited by IVM in G36'M GABACls (Fig. 14B and C). Currents induced by the EC_{90} (300 μM) of GABA were also not inhibited by IVM in G36'A GABACls (Fig. 14B).

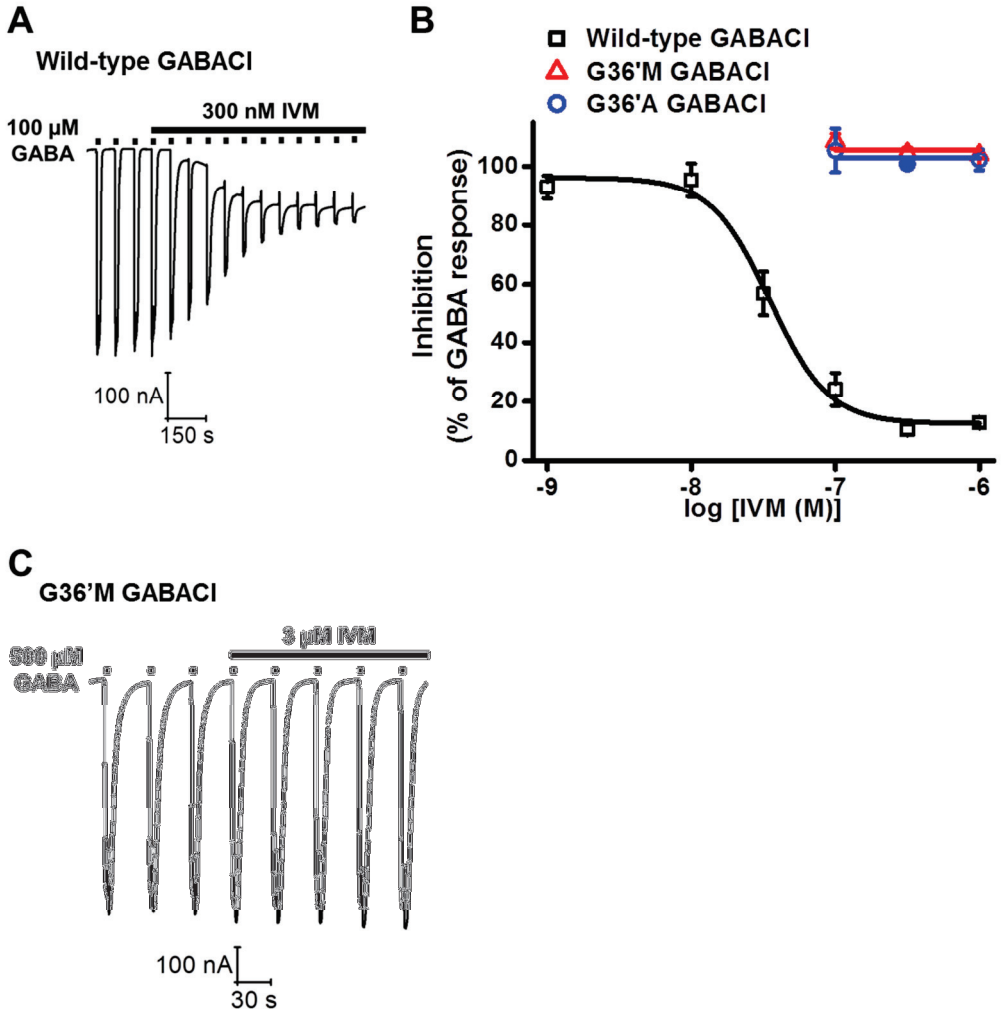

Fig. 14. IVM inhibition of EC_{90} GABA-induced currents in wild-type, G36'M, and G36'A GABACls. (A) A current trace showing IVM inhibition of currents in wild-type GABACls. (B) IVM concentration-response curves for the inhibition of GABA-induced currents of wild-type, G36'M, and G36'A GABACls. Error bars indicate SEM (n=6). (C) A current trace showing the effects of IVM on GABA-induced currents in G36'M GABACls.

Actions of IVM on GluCls

It was examined whether IVM activates *Musca* wild-type GluCls to elicit inward currents through the channels. Application of IVM alone to wild-type GluCls expressed in *Xenopus* oocytes for 3 min elicited sustained currents (Fig. 15A and B), with an EC_{50} of 6.79 ± 1.48 nM (Fig. 15B). In contrast to the wild type, G36'M GluCl was not activated by IVM even when tested at high concentrations (Fig. 15B and C).

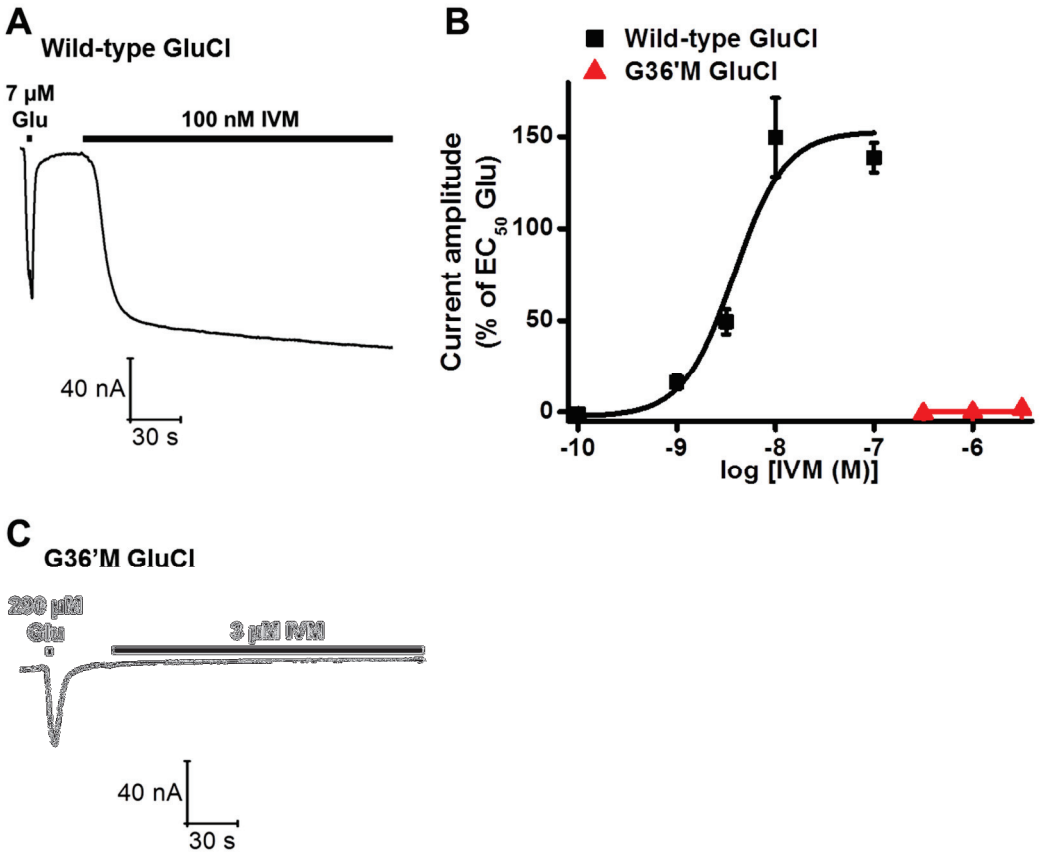

Fig. 15. IVM activation of wild-type and G36'M GluCls. (A) A trace current induced by IVM administered to wild-type GluCls. (B) IVM concentration-response curves for the activation of wild-type and G36'M GluCls. Error bar indicate SEM (n=6-8). (C) A current trace when IVM was administered to G36'M GluCls.

The IVM potentiation of Glu-induced currents in *Musca* GluCls was then examined. The amplitude of currents induced by the EC_5 (0.3 μM) of Glu was increased by the perfusion of IVM in wild-type GluCls; the EC_{50} of IVM was 13.5 ± 3.8 nM (Fig. 16A and B). The EC_{50} of IVM for the potentiation in GluCls was 3.5-fold smaller than that in GABACls ($p < 0.01$). Simultaneously, a slow current induced by IVM became prominent (Fig. 16A) in the wild-type GluCls. Although the potentiation of currents induced by the EC_5 (10 μM) of Glu was also observed in G36'M GluCls, a higher concentration of IVM (> 1 μM) was required than the concentration needed in wild-type GluCls (Fig. 16B and C).

In contrast to the potentiation with the EC_5 of Glu, currents induced by the EC_{90} (30 μM) of Glu were inhibited by the perfusion of IVM in wild-type GluCls; the IC_{50} of IVM was 4.92 ± 2.23 nM, which is 8.5-fold smaller than that in wild-type GABACls (*p*

< 0.01) (Fig. 17A and B, Table 3). In G36'M GluCls, currents induced by the EC_{90} (1 mM) of Glu were not inhibited but potentiated by the perfusion of IVM, with an EC_{50} of 603 ± 89 nM (Fig. 17C and D).

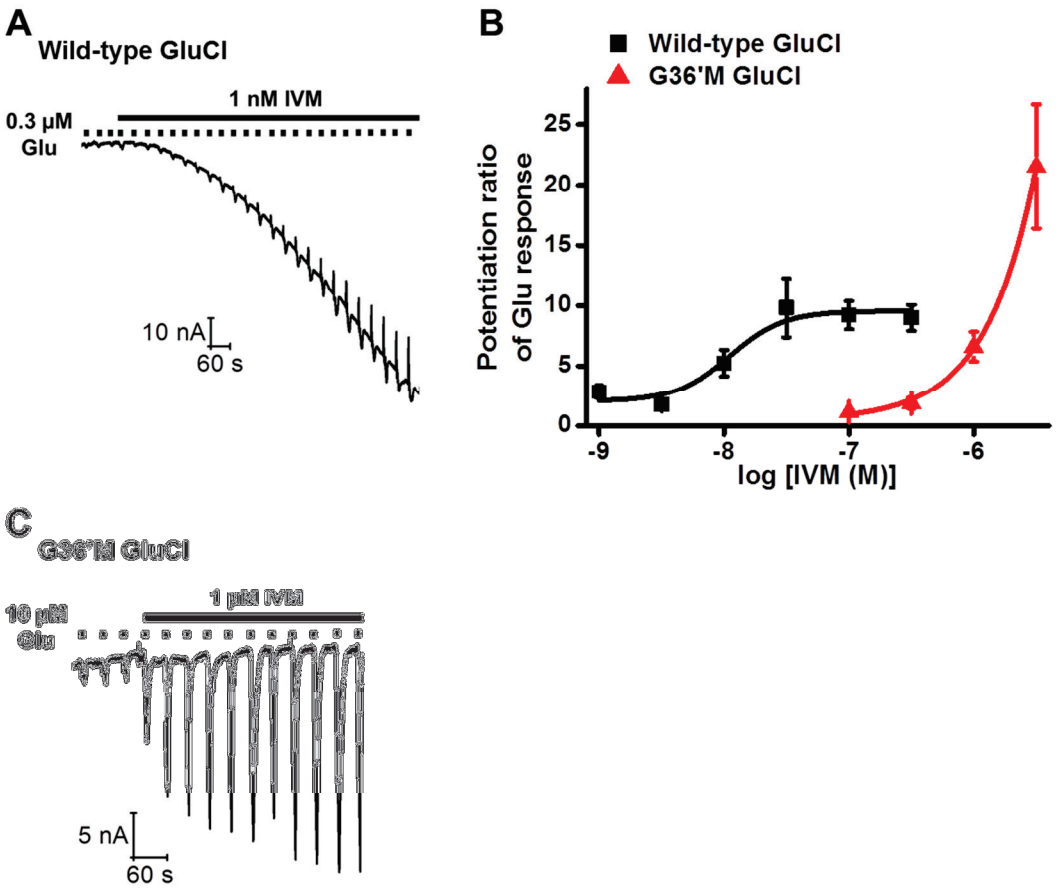

Fig. 16. IVM potentiation of EC_5 Glu-induced currents in wild-type and G36'M GluCls. (A) A current trace showing the IVM potentiation of currents in wild-type GluCls. (B) IVM concentration-response curves for the potentiation of Glu-induced currents in wild-type and G36'M GluCls. Error bars indicate SEM (n=6-9). (C) A current trace showing the IVM potentiation of currents in G36'M GluCls.

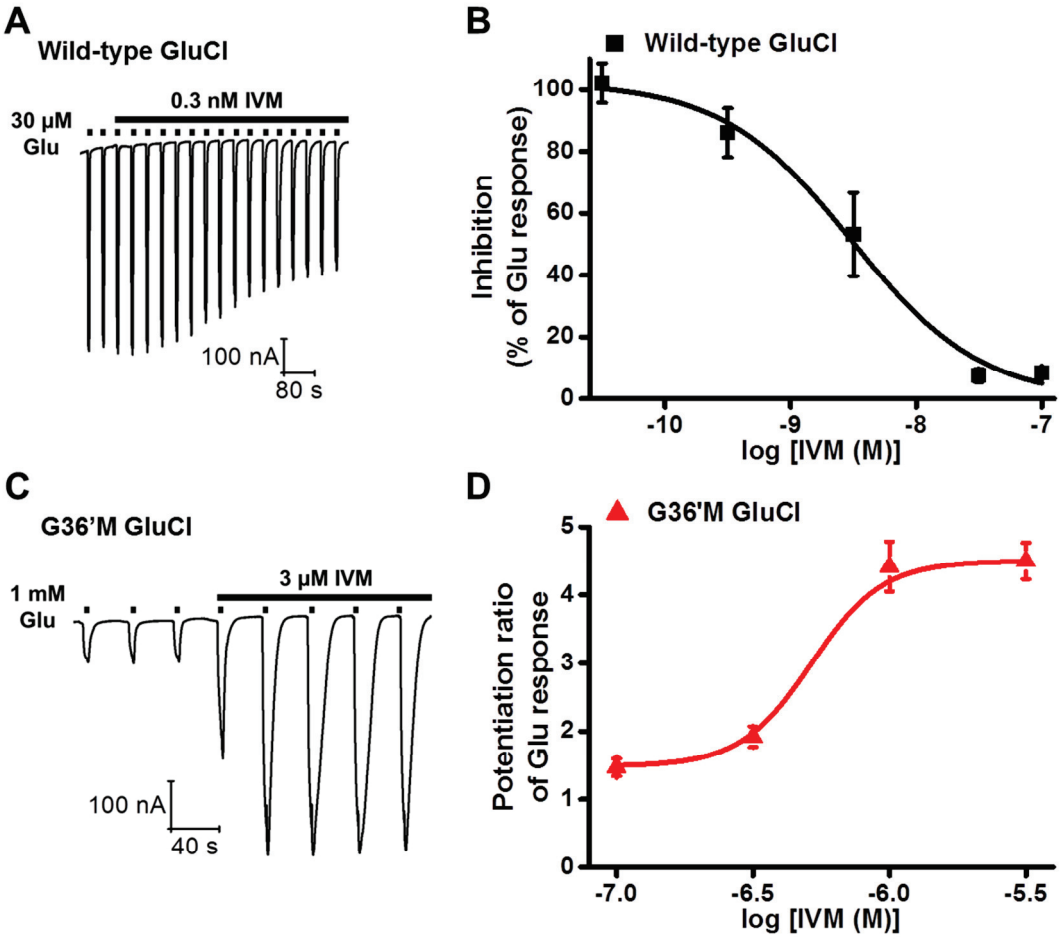

Fig. 17. IVM inhibition of EC_{90} Glu-induced currents in wild-type and G36'M GluCls. (A) A current trace showing the IVM inhibition of currents in wild-type GluCls. (B) IVM concentration-response curves for the inhibition of Glu-induced currents in wild-type GluCls. Error bars indicate SEM (n=6). (C) A current trace showing the IVM potentiation of currents in G36'M GluCls. (D) IVM concentration-response curves for the potentiation of Glu-induced currents in G36'M GluCls. Error bars indicate SEM (n=6).

Table 3. Potencies of IVM in the activation, potentiation, and antagonism of *Musca* GluCls and GABACls.

		Activation (EC_{50})[a]	Potentiation (EC_{50})[b]	Inhibition (IC_{50})[c]
GluCls	Wild-type	6.79 ± 1.48 nM	13.5 ± 3.8 nM	4.92 ± 2.23 nM
	G312M	NR[d]	>3 μM	603 ± 89 nM[e]
GABACls	Wild-type	1.25 ± 0.40 μM	46.6 ± 1.9 nM	42.0 ± 7.7 nM
	G333M	NR[d]	NR[d]	NR[d]
	G333A	>3 μM	294 ± 47 nM	NR[d]

Data are the mean of at least 6 experiments ± SEM

[a] Application of IVM alone.

[b] Application of agonist (EC_5) with perfusion of IVM.

[c] Application of agonist (EC_{90}) with perfusion of IVM.

[d] NR, no response.

[e] EC_{50} of the IVM potentiation.

Discussion

The housefly (*M. domestica*) that is capable of carrying over 100 pathogens has spread all over the world (Malik et al., 2007). The studies on the housefly are important in terms of controlling insect pests. First, we examined the insecticidal effect of IVM against adult female houseflies. The toxic symptom that IVM caused immobilization in flies, followed by death, suggested that the effects of IVM on houseflies are related to the activation of inhibitory neurotransmitter receptors.

The present study results indicate that IVM with high insecticidal activity against the housefly exerts unique triple effects (activation, potentiation, and antagonism) on both *Musca* GluCls and GABACls expressed in *Xenopus* oocytes. It has been previously reported that *Musca* GluCls were activated by a 10-s application of 500 nM IVM, whereas *Musca* GABACls were not activated (Eguchi et al, 2006). However, when IVM was perfused for a longer time on oocytes expressing wild-type *Musca* GABACls, IVM elicited slow, sustained currents (Fig. 11A). The EC_{50} of IVM in activating *Musca* GABACls was almost similar to that (2.3 μM) in rat α1β2γ2S GABACls (Adelsberger et al., 2000). In the activation by IVM, wild-type GluCls were 184-fold more sensitive than wild-type GABACls (Fig. 11B, Fig. 15B, Table 3). The X-ray crystallographic analysis revealed that when IVM binds to the *C. elegans* GluCl-α channel, it forms hydrogen bonds with S260 (15') in TM2 and T285 (40') in TM3 in the subunit interface

(Hibbs and Gouaux, 2011). These polar amino acids are conserved or conservatively substituted by hydrophilic amino acids in the *Musca* GluCl subunit but are substituted with Met and Val, respectively, in the *Musca* GABACl Rdl subunit (Fig. 2C). These changes in amino acids might result in the lower potency of IVM in *Musca* GABACls.

Aside from activation, it was shown that IVM potentiates currents induced by concentrations of GABA below its EC_{50} in wild-type GABACls, whereas it inhibits currents induced by concentrations of GABA above its EC_{50} (Fig. 12). IVM does the same in GluCls as in GABACls in this respect (Fig. 16A and B, Fig. 17A and B). IVM was reported to act as an antagonist in GABACls containing *Drosophila* Rdl_{bd} subunits when co-applied with 100 μM GABA (above EC_{50}) (Lees et al, 2014), whereas IVM alone acted as an allosteric agonist in *Drosophila* GABACls composed of the same Rdl_{bd} subunits (Nakao et al., 2015). In native GABACls in mouse hippocampal embryonic neurons, IVM induced small currents and potentiated currents induced by low concentrations of GABA with an EC_{50} of 17.8 nM, whereas it inhibited currents induced by high concentrations of GABA (Krůšek and Zemková, 1994). In *Drosophila* GluCls, currents induced by 10 μM Glu were slightly (only 24%) potentiated after pretreatments with 1 nM IVM phosphate, whereas currents elicited by 300 μM Glu were not significantly altered (Cully et al., 1996). The Glu response was 49% reduced by 10 nM $IVMPO_4$. The potentiation and antagonism are less prominent compared with the activation in *Drosophila* GluCls. Our data clearly indicate that whether IVM induces potentiation or antagonism in GluCls and GABACls depends on agonist concentrations (Fig. 12).

It was observed that the IVM potentiates currents induced by the EC_5 of Glu or GABA and that IVM inhibits currents induced by the EC_{90} of Glu or GABA in wild-type GluCls and GABACls. The EC_{50} of IVM for the potentiation in GluCls was 3.5-fold smaller than that in GABACls (Fig. 13B, Fig. 16B, Table 3), and the IC_{50} of IVM for the inhibition in GluCls is 8.5-fold smaller than that in GABACls (Fig. 14B, Fig. 17B, Table 3). Thus, GluCls are also more sensitive to IVM than GABACls in these actions. When IVM potentiates agonist-induced currents in both receptors, it is worth noting that the potentiation seems to be accompanied by the elicitation of slow, sustained currents by IVM itself and the diminishment of Glu- or GABA-induced currents at a later stage as exemplified by currents traces in Figures 13A and 16A. This suggests that IVM might change the interacting amino acid residues by moving inward in the crevice during channel activation.

The amino acids at the 36’ position in TM3 (Fig. 2C), are likely one of the most important residues for the action of IVM as the equivalent amino acid residues were

reported to be essential for IVM actions in Cys-loop receptors (Lynagh and Lynch, 2010). Therefore it was examined how the substitution of G36' affects the three actions of IVM. The Met mutants, G36'M GluCl and G36'M GABACl, did not undergo activation provoked by IVM. However, a diminished activation was observed in G36'A GABACls, resulting in a decrease in the potency of IVM. As the interaction of IVM with the 15' amino acid in TM2 is required for the activation of channels (Hibbs and Gouaux, 2011), bulky side-chain amino acids at the entrance of the IVM binding crevice might destabilize or inhibit the binding of IVM to the position of the 15' amino acid. Currents induced by the EC_5 of Glu were potentiated in G36'M GluCls, albeit by high concentrations of IVM. G36'M GABACls showed little potentiation of EC_5 GABA-induced currents even with the perfusion of high concentrations of IVM. GABACls are more affected by the steric hindrance at the 36' position in potentiation compared with GluCls. However, G36'A GABACls showed greater potentiation but a decrease in the potency of IVM compared with wild-type GABACls during the perfusion of high concentrations of IVM. The maximum amplitude of the potentiation of GABA-induced currents in G36'A GABACls was 6.7-fold greater compared with that of wild-type GABACls. However, this is most likely because these mutant channels do not undergo the diminishment or antagonism of GABA-induced currents by IVM, which occurs in wild-type GABACls at a later stage of response (Fig. 13A, 14B, C). Although G36'M and G36'A GABACls did not undergo IVM antagonism of currents induced by high concentrations of GABA, G36'M GluCls exhibited the IVM potentiation of currents induced by high concentrations of Glu rather than the antagonism. It remains to be investigated whether this peculiar action of G36'M GluCls is associated with the agonist profile, such as a small Hill coefficient, in this mutant. Piecing together, these findings indicate that G36' at the entrance of the IVM binding crevice play crucial roles in IVM activation, potentiation, and antagonism in GluCls and GABACls. Of these effects, the antagonism seems to be most critically affected by the 36' amino acid as it was abolished by mutations.

In α1β2γ2L GABACls, IVM binding to non-equivalent intersubunit sites with different interacting amino acids has been shown to induce different conformational states leading to the activation, potentiation, and inhibition of currents (Estrada-Mondragon and Lynch, 2015). In the case of homo-pentameric channels such as *Musca* GluCls and GABACls, there are five equivalent binding sites for IVM, given that IVM binds to intersubunit crevices. It was shown in the present study that whether IVM potentiates or inhibits agonist-induced currents depends on agonist concentrations. In homo-pentamers, which have five orthosteric binding sites, global structural changes

to produce an open state of a channel differ by how many agonists bind to the orthosteric sites. (Rayes et al., 2009). The findings presented in this chapter may indicate that the binding of IVM to its binding sites with different conformations, which are induced by different concentrations of agonists, leads to potentiation or antagonism of agonist-induced currents.

Chapter 4

Conclusion

IVM is an antiparasitic agent against parasitic worms and arthropods. This agent is effectively used to treat river blindness caused by infection with *Onchocerca* sp. (Campbell W.C., 1982). IVM was previously defined as a positive allosteric modulator for GluCls. Apart from this definition, a variety of actions on ion channels were revealed to date. These actions include the activation, potentiation, and antagonism of ion channels. It is important to identify the molecular site of action and mechanism.

In the present study, three photoreactive IVM analogues, **PP1-3**, in which the dioleandrosyl group of IVM B_{1a} was replaced with photoreactive functional groups, were synthesized to chemically identify the IVM-binding site in GluCls. [^{3}H]IVM B_{1a}-binding assays and functional TEVC assays using Hco-AVR-14B-GluCls indicated that the three photoreactive probes have the low- or subnanomolar affinity for the Hco-AVR-14B-GluCls and *Bombyx*/*D*-GluCls. Of the three probes, **PP2** has the highest affinity and sensitivity for Hco-AVR-14B-GluCls.

To introduce ^{125}I into **PP2**, **IodoPP2** was synthesized and tested for the affinity for Hco-AVR-14B-GluCls using [^{3}H]IVM B_{1a}-binding assay. **IodoPP2** has an affinity similar to that of **PP2**. **[^{125}I]IodoPP2** was synthesized from **IodoPP2** using the chloramine-T method, and used for the photolabeling of Hco-AVR-14B-GluCls solubilized from oocyte membranes. However, **[^{125}I]IodoPP2** was found not to label GluCls. It was speculated that the photoreactive group of **IodoPP2** was located outside of Hco-AVR-14B-GluCls when it binds to GluCls. These results indicate that a photoreactive group should be introduced near the macrolactone ring.

IVM modulates not only GluCls but also various ion channels and exerts various effects on each channel. Electrophysiological analyses were made to clarify what type of action of IVM on *Musca* GluCls or GABACls plays major roles in the manifestation of their insecticidal effects. When *Musca* GluCls were treated with IVM B_{1a} for 10s, *Musca* GABACls were not activated (Eguchi et al., 2006). However, the present study showed that IVM activated *Musca* GABACls by a 3-min application. In this action, *Musca* GluCls were more sensitive to IVM than *Musca* GABACls. Aside from the activation, IVM potentiated currents induced by lower concentrations of GABA than its EC_{50} in *Musca* GABACls, and it inhibited currents induced by concentrations of GABA

above its EC_{50}. It was also examined whether the same effects of IVM were also observed on *Musca* GluCls. IVM was shown to potentiate currents induced by the EC_5 of Glu and GABA and inhibit currents induced by the EC_{90} of Glu in *Musca* GluCls. Also in these actions, *Musca* GluCls were more sensitive to IVM than *Musca* GABACls.

The glycine at the 36' position in TM3 was reported to play a key role in IVM binding to various Cys-loop receptors. In the present study, the triple actions of IVM B_{1a} were examined in the G36' mutants of *Musca* GluCls (G36'M *Musca* GluCls) and *Musca* GABACls (G36'M and G36'A *Musca* GABACls). IVM activation disappeared in G36'M *Musca* GluCls and *Musca* GABACls, although diminished activation was observed in G36'A *Musca* GABACls. IVM potentiation of EC_5 agonist-induced currents was seen with lower potencies in G36'M *Musca* GluCls and G36'A *Musca* GABACls, but was not maintained in G36'M *Musca* GABACls. In the three mutants, IVM inhibition of EC_{90} agonist-induced currents was not observed. Overall, these findings indicate that *Musca* GluCls are the primary target of IVM triple actions and that IVM triple actions occur by binding to the binding site in the TM1-TM3 subunit interface.

In conclusion, three photoaffinity probes were synthesized to identify the IVM-binding site of GluCls. Although these probes had high affinity for GluCls, a ^{125}I-labeled probe failed to covalently bind to GluCls. Although these results are disappointing, they offer future prospects for synthesizing improved probes. Electrophysiological analysis of IVM actions were performed to define the molecular mechanism of action of IVM using wild-type and mutant *Musca* GluCls and GABACls. These analyses showed that IVM exhibited a triple action (activation, potentiation, and antagonism) on both GluCls and GABACls. In these actions, GluCls were more sensitive to IVM than GABACls, indicating that GluCls are a primary target of IVM. The results presented in this thesis provide invaluable information about the development of new pest control agents.

Acknowledgements

First, and foremost, I would like to express my gratitude to my advisor, Dr. Yoshihisa Ozoe, Professor, Department of Life Science and Biotechnology, Faculty of Life and Environmental Science, Shimane University, for his guidance and warm encouragement throughout my study.

I also thank Dr. Hiromitsu Nakajima, Trustee (Research and Environment) and Vice-President, Tottori University, for his warm encouragement and advices.

Furthermore, I would like to thank Dr. Izumi Ikeda, Associate Professor, Shimane University, and Dr. Kenjiro Furuta, Assistant Professor, Shimane University, for their advices about organic chemistry and various techniques. I am also indebted to Ms. Fumiyo Ozoe, senior researcher, for various discussions.

Finally, I would like to take an opportunity to thank Dr. Tomo Kita and all other lab members for their cooperation.

References

Adelsberger, H., Lepier, A., Dudel, J., 2000. Activation of rat recombinant $\alpha_1\beta_2\gamma_{2S}$ $GABA_A$ receptor by the insecticide ivermectin. Eur. J. Pharmacol. 394, 163-170.

Althoff, T., Hibbs, R.E., Banerjee, S., Gouaux, E., 2014. X-ray structures of GluCl in apo states reveal a gating mechanism of Cys-loop receptors. Nature 512, 333-337.

Arena, J.P., Liu, K.K., Paress, P.S., Frazier, E.G., Cully, D.F., Mrozik, H., Schaeffer, J.M., 1995. The mechanism of action of avermectins in *Caenorhabditis elegans*: correlation between activation of glutamate-sensitive chloride current, membrane binding, and biological activity. J. Parasitol. 81, 286-294.

Blizzard, T.A., Margiatto, G.M., Mrozik, H., Shoop, W.L., Frankshun, R.A., Fisher, M.H., 1992. Synthesis and biological activity of 13-*epi*-avermectins: potent anthelmintic agents with an increased margin of safety. J. Med. Chem. 35, 3873-3878.

Bradford, M.M., 1976. A rapid and sensitive method for the quantitation of microgram quantities of protein utilizing the principle of protein-dye binding. Anal. Biochem. 72, 248-254.

Buckingham, S.D., Biggin, P.C., Sattelle, B.M., Brown, L.A., Sattelle, D.B. 2005. Insect GABA receptors: splicing, editing, and targeting by antiparasitics and insecticides. Mol. Pharmacol. 68, 942-951.

Burg, R.W., Miller, B.M., Baker, E.E., Birnbaum, J., Currie, S.A., Hartman, R., Kong, Y.-L., Monaghan, R.L., Olson, G., Putter, I., Tunac, J.B., Wallick, H., Stapley, E.O., Ōiwa, R., Ōmura, S., 1979. Avermectins, new family of potent anthelmintic agents: producing organism and fermentation. Antimicrob. Agents Chemother. 15, 361-367.

Campbell, W.C., 1982. Efficacy of the avermectins against filarial parasites: a short review. Vet. Res. Commun. 5, 251-262

Charnet, P, Labarca, C., Leonard, R.J., Vogelaar, N.J., Czyzyk, L., Gouin, A., Davidson, N., Lester, H.A., 1990. An open-channel blocker interacts with adjacent turns of α-helices in the nicotinic acetylcholine receptor. Neuron 4, 87-95.

Cheeseman, C.L., Delany, N.S., Woods, D.J., Wolstenholme, A.J., 2001. High-affinity ivermectin binding to recombinant subunits of the *Haemonchus contortus* glutamate-gated chloride channel. Mol. Biochem. Parasitol. 114, 161-168.

Cheng, Y-C., Prusoff, W.H., 1973. Relationship between the inhibition constant (*Ki*)

and the concentration of inhibitor which causes 50 per cent inhibition (I_{50}) of an enzymatic reaction. Biochem. Pharmacol. 22, 3099-3108.

Cully, D.F., Vassilatis, D.K., Liu, K.K., Paress, P.S., Van der Ploeg, L.H.T., Schaeffer, J.M., Arena, J.P., 1994. Cloning of an avermectin-sensitive glutamate-gated chloride channel from *Caenorhabditis elegans*. Nature 371, 707-711.

Cully, D.F., Paress, P.S., Liu, K.K., Schaeffer, J.M., Arena, J.P., 1996. Identification of a *Drosophila melanogaster* glutamate-gated chloride channel sensitive to the antiparasitic agent avermectin. J. Biol. Chem. 271, 20187-20191.

Dawson, G.R., Wafford, K.A., Smith, A., Marshall, G.R., Bayley, P.J., Schaeffer, J.M., Meinke, P.T., Mckernan, R.M., 2000. Anticonvulsant and adverse effects of avermectin analogs in mice are mediated through the γ-aminobutyric $acid_A$ receptor. J. Pharmacol. Exp. Ther. 295, 1051-1060.

Démares, F., Raymond, V., Armengaud, C., 2013. Expression and localization of glutamate-gated chloride channel variants in honeybee brain (*Apis mellifera*). Insect Biochem. Mol. Biol. 43, 115-124.

Dent, J.A., Smith, M.M., Vassilatis, D.K., Avery, L., 2000. The genetics of ivermectin resistance in *Caenorhabditis elegans*. Proc. Natl. Acad. Sci. USA 97, 2674-2679.

Dermauw, W., Ilias, A., Riga, M., Tsagkarakou, A., Grbić, M., Tirry, L., Van Leeuwen, T., Vontas, J., 2012. The cys-loop ligand-gated ion channel gene family of *Tetranychus urticae*: implications for acaricide toxicology and a novel mutation associated with abamectin resistance. Insect Biochem. Mol. Biol. 42, 455-465.

Duce, I.R., Scott, R.H.,1985. Actions of dihydroavermectin B_{1a} on insect muscle. Br. J. Pharmacol. 85, 395-401.

Eguchi, Y., Ihara, M., Ochi, E., Shibata, Y., Matsuda, K., Fushiki, S., Sugama, H., Hamasaki, Y., Niwa, H., Wada, M., Ozoe, F., Ozoe, Y., 2006. Functional characterization of *Musca* glutamate- and GABA-gated chloride channels expressed independently and coexpressed in *Xenopus* oocytes. Insect Mol. Biol. 15, 773-783.

Estrada-Mondragon, A., Lynch, J.W., 2015. Functional characterization of ivermectin binding sites in α1β2γ2L GABA(A) receptors. Front. Mol. Neurosci. 8:55

ffrench-Constant, R.H., Mortlock, D.P., Shaffer, C.D., MacIntyre, R.J., Roush, R.T., 1991. Molecular cloning and transformation of cyclodiene resistance in *Drosophila*: an invertebrate γ-aminobutyric acid subtype A receptor locus. Proc. Natl. Acad. Sci. USA 88, 7209-7213.

Forrester, S.G., Prichard, R.K., Beech, R.N., 2002. A glutamate-gated chloride channel subunit from *Haemonshus contortus*: expression in a mammalian cell line, ligand binding, and modulation of anthelmintic binding by glutamate. Biochem.

Pharmacol. 63, 1061-1068.

Glendinning, S.K., Buckingham, S.D., Sattelle, D.B., Wonnacott, S., Wolstenholme, A.J., 2011. Glutamate-gated chloride channels of *Haemonchus contortus* restore drug sensitivity to ivermectin resistant *Caenorhabditis elegans*. PLoS ONE 6, e22390.

Harrison, J.B., Chen, H.H., Sattelle, E., Barker, P.J., Huskisson, N.S., Rauh, J.J., Bai, D., Sattelle, D.B., 1996. Immunocytochemical mapping of a C-terminus anti-peptide antibody to the GABA receptor subunit, RDL in the nervous system of *Drosophila melanogaster*. Cell Tissue Res. 284:269-278.

Hibbs, R.E., Gouaux, E., 2011. Principles of activation and permeation in an anion-selective Cys-loop receptor. Nature 474, 54-60.

Horenstein, J., Wagner, D.A., Czajkowski, C., Akabas, M.H., 2001. Protein mobility and GABA-induced conformational changes in $GABA_A$ receptor pore-lining M2 segment. Nat. Neurosci. 4, 477-485.

Khakh, B.S., Proctor, W.R., Dunwiddie, T.V., Labarca, C., Lester, H.A., 1999. Allosteric control of gating and kinetics at $P2X_4$ receptor channels. J. Nurosci. 19, 7289-7299.

Kita, T., Ozoe, F., Azuma, M, Ozoe, Y., 2013. Differential distribution of glutamate- and GABA-gated chloride channels in the housefly *Musca domestica*. J. Insect Physiol. 59, 887-893.

Kita, T., Ozoe, F., Ozoe, Y., 2014. Expression pattern and function of alternative splice variants of glutamate-gated chloride channel in the housefly *Musca domestica*. Insect Biochem. Mol. Biol. 45, 1-10.

Krause, R.M., Buisson, B., Bertrand, S., Corringer, P.-J., Galzi, J.-L., Changeux, J.-P., Bertrand, D., 1998. Ivermectin: a positive allosteric effector of the α7 neuronal nicotinic acetylcholine receptor. Mol. Pharmacol. 53, 283-294.

Krůšek, J., Zemková, H., 1994. Effect of ivermectin on γ-aminobutyric acid-induced chloride currents in mouse hippocampal embryonic neurons. Eur. J. Pharmacol. 259, 121-128.

Kwon, D.H., Yoon, K.S., Clark, J.M., Lee, S.H., 2010. A point mutation in a glutamate-gated chloride channel confers abamectin resistance in the two-spotted spider mite, *Tetranychus urticae* Koch. Insect Mol. Biol. 19, 583-591.

Lapatsanis, L., Milias, G., Froussios, K., Kolovos, M., 1983. Synthesis of *N*-2,2,2-(trichloroethoxycarbonyl)-L-amino acids and *N*-(9-fluorenylmethoxycarbonyl)-L-amino acids involving succinimidoxy anion as a leaving group in amino acid protection. Synthesis 8, 671-673.

Lasota, J.A., Dybas, R.A., 1991. Avermectins, a novel class of compounds: implications for use in arthropod pest control. Annu. Rev. Entomol. 36, 91-117.

Lees, K., Musgaard, M., Suwanmanee, S., Buckingham, S.D., Biggin, P., Sattelle, D., 2014. Actions of agonists, fipronil and ivermectin on the predominant *in vivo* splice and edit variant (RDL_{bd}, I/V) of the *Drosophila* GABA receptor expressed in *Xenopus laevis* oocytes. PLoS One 9, e97468.

Liu, W.W., Wilson, R.I., 2013. Glutamate is an inhibitory neurotransmitter in the *Drosophila* olfactory system. Proc. Natl. Acad. Sci. USA 110, 10294-10299.

Lynagh, T., Lynch, J.W., 2010. A glycine residue essential for high ivermectin sensitivity in Cys-loop ion channel receptors. Int. J. Parasitol. 40, 1477-1481.

Malik, A., Singh, N., Satya, S., 2007. House fly (*Musca domestica*): A review of control strategies for a challenging pest. J. Environ. Sci. Heal. B 42, 453-469.

McCavera, S., Rogers, A.T., Yates, D.M., Woods, D.J., Wolstenholme, A.J., 2009. An ivermectin-sensitive glutamate-gated chloride channel from the parasitic nematode *Haemonchus contortus*. Mol. Pharmacol. 75, 1347-1355.

McTier, T.L., Chubb, N., Curtis, M.P., Hedges, L., Inskeep, G.A., Knauer, C.S., Menon, S., Mills, B., Pullins, A., Zinser, E., Woods, D.J., Meeus, P., 2016. Discovery of sarolaner: A novel, orally administered, broad-spectrum, isoxazoline ectoparasiticide for dogs. Vet. Parasitol. 222, 3-11.

Meinke, P.T., Rohrer, S.P., Hayes, E.C., Schaeffer, J.M., Fisher, M.H., Mrozik, H., 1992. Affinity probes for the avermectin binding proteins. J. Med. Chem. 35, 3879-3884.

Miller, P.S., Aricescu, A.R., 2014. Crystal structure of a human $GABA_A$ receptor. Nature 512, 270-275.

Mrozik, H., Eskola, P., Arison, B.H., Albers-Schönberg, G., Fisher, M.H., 1982. Avermectin aglycons. J. Org. Chem. 47, 489-492

Nakao, T., Banba, S., 2016. Broflanilide: a meta-diamide insecticide with a novel mode of action. Bioorg. Med. Chem. 24, 372-377.

Nakao, T., Banba, S., Hirase, K., 2015. Comparison between the modes of action of novel meta-diamide and macrocyclic lactone insecticides on the RDL GABA receptor. Pestic. Biochem. Physiol. 120, 101-108.

Olsen, R.W., Sieghart, W., 2008. International union of pharmacology. LXX. Subtypes of γ-aminobutyric $acid_A$ receptors: classification on the basis of subunit composition, pharmacology, and function. Update. Pharmacol. Rev. 60, 243-260.

Õmura, S., Crump, A., 2004. The life and times of ivermectin - a success story. Nat. Rev. Microbiol. 2, 984-989.

Ozoe, Y., 2013. γ-Aminobutyrate- and glutamate-gated chloride channels as targets of insecticides. Adv. Insect Physiol. 44, 211-286.

Ozoe, Y., Asahi, M., Ozoe, F., Nakahira, K., Mita, T., 2010. The antiparasitic isoxazoline A1443 is a potent blocker of insect ligand-gated chloride channels. Biochem. Biophys. Res. Commun. 391, 744-749.

Ozoe, Y., Kita, T., Ozoe, F., Nakao, T., Sato, K., Hirase, K., 2013. Insecticidal 3-benzamido-*N*-phenylbenzamides specifically bind with high affinity to a novel allosteric site in housefly GABA receptors. Pestic. Biochem. Physiol. 107, 285-292.

Rayes, D., De Rosa, M.J., Sine, S.M., Bouzat, C., 2009. Number and locations of agonist binding sites required to activate homomeric Cys-Loop receptors. J. Neurosci. 29, 6022-6032.

Raymond, V., Sattelle, D.B., 2002. Novel animal-health drug targets from ligand-gated chloride channels. Nat. Rev. Drug. Discov. 1, 427-436.

Remnant, E.J., Good, R.T., Schmidt, J.M., Lumb, C., Robin, C., Daborn, P.J., Batterham, P., 2013. Gene duplication in the major insecticide target site, *Rdl*, in *Drosophila melanogaster*. Proc. Natl. Acad. Sci. USA 110, 14705-14710.

Rohrer, S.P., Birzin, E.T., Costa, S.D., Arena, J.P., Hayes, E.C., Schaeffer, J.M., 1995. Identification of neuron-specific ivermectin binding sites in *Drosophila melanogaster* and *Schistocerca americana*. Insect Biochem. Mol. Biol. 25, 11-17.

Rohrer, S.P., Jacobson, E.B., Hayes, E.C., Birzin, E.T., Schaeffer, J.M., 1994. Immunoaffinity purification of avermectin-binding proteins from the free-living nematode *Caenorhabditis elegans* and the fruitfly *Drosophila melanogaster*. Biochem. J. 302, 339-345.

Rohrer, S.P., Meinke, P.T., Hayes, E.C., Mrozik, H., Schaeffer, J.M., 1992. Photoaffinity labeling of avermectin binding sites from *Caenohabditis elegans* and *Drosophila melanogaster*. Proc. Natl. Acad. Sci. USA 89, 4168-4172.

Scatchard, G., 1949. The attractions of proteins for small molecules and ions. Ann. N. Y. Acad. Sci. 51, 660-672.

Scott, R.H., Duce, I.R., 1985. Effects of 22,23-dihydroavermectin B_{1a} on locust (*Schistocerca gregaria*) muscles may involve several sites of action. Pest Manag. Sci. 16, 599-604

Shan, Q., Haddrill, J.L., Lynch, J.W., 2001. Ivermectin, an unconventional agonist of the glycine receptor chloride channel. J. Biol. Chem. 276, 12556-12564.

Shoop, W.L., Mrozik, H., Fisher, M.H., 1995. Structure and activity of avermectins and milbemycins in animal health. Vet. Parasitol. 59, 139-156.

Shoop, W.L., Hartline, E.J., Gould, B.R., Waddell, M.E., McDowell, R.G., Kinney, J.B.,

Lahm, G.P., Long, J.K., Xu, M., Wagerle, T., Jones, G.S., Dietrich, R.F., Cordova, D., Schroeder, M.E., Rhoades, D.F., Benner, E.A., Confalone, P.N., 2014. Discovery and mode of action of afoxolaner, a new isoxazoline parasiticide for dogs. Vet. Parasitol. 201, 179-189.

Sigel, E., Baur, R., 1987. Effect of avermectin B_{1a} on chick neuronal γ-aminobutyrate receptor channels expressed in *Xenopus* oocytes. Mol. Pharmacol. 32, 749-752.

Smart, T.G., Paoletti, P., 2012. Synaptic neurotransmitter-gated receptors. Cold Spring Harb. Perspect. Biol. 4, a009662.

Tsukamoto, Y., Cole, L.M., Casida, J.E., 2000. Avermectin chemistry and action: ester- and ether-type candidate photoaffinity probes. Bioorg. Med. Chem. 8, 19-26.

Yamaguchi, M., Sawa, Y., Matsuda, K., Ozoe, F., Ozoe, Y., 2012. Amino acid residues of both the extracellular and transmembrane domains influence binding of the antiparasitic agent milbemycin to *Haemonchus contortus* AVR-14B glutamate-gated chloride channels. Biochem. Biophys. Res. Commun. 419, 562-566.

Zemkova, H., Tvrdonova, V., Bhattacharya, A., Jindrichova, M., 2014. Allosteric modulation of ligand gated ionchannels by ivermectin. Physiol. Res. 63 (Suppl. 1), S215-S224.

List of Publication

Chapter 2

Fuse, T., Ikeda, I., Kita, T., Furutani, S., Nakajima, H., Matsuda, K., Ozoe, F., Ozoe, Y., 2015. Synthesis of photoreactive ivermectin B_{1a} derivatives and their actions on *Haemonchus* and *Bombyx* glutamate-gated chloride channels. Pestic. Biochem. Physiol. 120, 82-90.

Chapter 3

Fuse, T., Kita, T., Nakata, Y., Ozoe, F., Ozoe, Y., 2016. Electrophysiological characterization of ivermctin triple actions on *Musca* chloride channels gated by L-glutamic acid and γ-aminobutyric acid. Insect Biochem. Mol. Biol. 77, 78-86.

Summary

L-Glutamic acid (Glu) and γ-aminobutyric acid (GABA) are the major neurotransmitters that exert excitatory and inhibitory effects, respectively, on neurotransmission in vertebrates. In invertebrate, Glu and GABA exert inhibitory effects by binding to Glu- and GABA-gated chloride channels (GluCls, GABACls), although Glu also has excitatory effects. GluCls are present only in invertebrates, and invertebrate GABACls differ from vertebrate GABACls in their subunit composition; therefore, these channels are major targets of insecticides and anthelmintics.

Ivermectin (IVM) is synthesized from avermectins that are produced by *Streptomyces avermitilis*, and IVM reportedly exerts insecticidal activities by acting on GluCls. The X-ray crystallographic analysis and site-directed mutagenesis studies of GluCls suggested that IVM binds at the transmembrane interface between TM1 to TM3. However, identification of the IVM-binding site by chemical means has yet to be achieved.

In this study, photoreactive IVM probes were synthesized and it was examined whether GluCls were photolabeled by the photoreactive probes. First, three photoreactive IVM probes (**PP1**-**3**), in which the dioleandrosyl moiety of IVM was replaced with different photoreactive substituents, were synthesized, and these probes were examined for their affinity for *Haemonchus contortus* GluCls (Hco-AVR-14B GluCls) and *Bombyx mori* GluCls (*Bombyx*/*D*-GluCls) using [^{3}H]IVM B_{1a} competition assays. Furthermore, the ability of these probes to activate GluCls was examined by two-electrode voltage clamp (TEVC) methods with Hco-AVR-14B GluCls. Of the three PPs, **PP2** was superior in both affinity and function at Hco-AVR-14B-GluCls. Next, **IodoPP2** was synthesized to prepare **[^{125}I]IodoPP2**, and it was confirmed that the affinity of **IodoPP2** does not differ from that of **PP2** using the [^{3}H]IVM B_{1a} assays with Hco-AVR-14B GluCls. Finally, **[^{125}I]IodoPP2** was synthesized from **IodoPP2** using the chloramine-T method. The photoaffinity labeling of Hco-AVR-14B-GluCls solubilized from oocyte membranes with the radiolabeled probe were performed. However, no specific cross-linked band of Hco-AVR-14B-GluCls was detected in the SDS gel. Nonetheless, these results provided clues as to the synthesis of improved probes.

IVM acts at various ion channels, but the molecular mechanism of action of IVM is not well defined. Therefore, the effects of IVM on housefly (*Musca domestica*) GluCls

and GABACls were examined. IVM elicited an irreversible response when applied alone to both channels. In this study, IVM itself induced currents in *Musca* GABACls by the administration for 3 min. In addition, *Musca* GluCls showed high sensitivity to IVM with 184-fold greater EC_{50} than *Musca* GABACls. The IVM potentiation and inhibition of currents induced by different concentration of GABA were examined in *Musca* GABACls. IVM potentiates currents induced by concentrations of GABA below its EC_{50}, whereas it inhibits current induced by concentrations of GABA above its EC_{50}. It was confirmed that the IVM potentiation of currents induced by the EC_5 of Glu or GABA and the IVM inhibition of currents induced by the EC_{90} of Glu or GABA were observed in *Musca* GluCls and GABACls. The sensitivity of IVM in both potentiation and inhibition in GluCls was higher than those in GABACls, indicating that IVM's primary target is GluCls as GluCls are more sensitive to IVM than GABACls in three actions.

Substitution of an amino acid residue at the 36' position of GluCls and GABACls resulted in significantly reduced levels or loss of IVM triple actions. Therefore, the glycine at the 36' position in TM3 is likely among the most important residues for the action of IVM. It is likely that these three actions result from the interaction of IVM with amino acid residues in the transmembrane intersubunit crevice.

Overall, the results presented in this thesis provide invaluable information about the development of new pest control agents.

要旨

L-グルタミン酸と γ-アミノ酪酸 (GABA) は代表的な神経伝達物質であり、脊椎動物ではそれぞれ興奮と抑制の神経制御に関わっている。この二つのアミノ酸は、無脊椎動物においてはグルタミン酸作動性クロルイオンチャネル (GluCl) および GABA 作動性クロルイオンチャネル (GABACl) にそれぞれ結合することによって抑制性の神経伝達を行っている (グルタミン酸は興奮性神経伝達物質でもある)。GluCl は無脊椎動物にしか存在が確認されておらず、また GABACl も脊椎動物とサブユニット構造が異なっていることから、いずれも害虫制御剤のターゲットとして注目されている。

イベルメクチン (IVM) は、放線菌 *Streptomyces avermitilis* より単離されたアベルメクチンの半合成駆虫薬であり、GluCl に特異的に結合することでチャネルを開口させ、駆虫作用を示すと考えられている。また、その結合部位についても X 線結晶構造解析や点変異試験により、M1-M3 サブユニットの間に結合することが報告されている。しかし、化学的手法を用いた結合部位の同定は未だ行われていない。

本研究では光反応性 IVM 類縁体を合成し、光親和性標識法で GluCl に対する IVM の結合部位の同定を試みた。まず初めに、IVM の 13 位のジオレアンドロシル基を、光反応基ベンゾイルアジドを持つ基質に置換することで 3 種類の光反応性 IVM 誘導体 (**PP1-3**) を合成し、捻転胃虫 *Haemonchus contortus* 由来の GluCl (Hco-AVR14B-GluCl) と *Bombyx mori* 由来の GluCl (*Bombyx*/*D*-GluCl) に対する [^{3}H]IVM B_{1a} 結合試験およびアフリカツメガエル卵母細胞に発現させた Hco-AVR14B-GluCl を用いた 2 電極膜電位固定 (TEVC) 法で親和性および活性を調べた。その結果、**PP2** が 3 種類の中で最も高い親和性および機能を持つことがわかった。次に標識部位として放射性ヨウ素 (^{125}I) 標識するため、**PP2** を基に **IodoPP2** を合成し、[^{3}H]IVM B_{1a} 試験を行って親和性が **PP2** と同等であることを確認した。**IodoPP2** からクロラミン T 法で**[^{125}I]IodoPP2** を合成した。合成した放射性 IVM 誘導体を用いて Hco-AVR14B-GluCl との光親和性標識を試みたが、特異的に標識されるバンドを SDS ゲル中に検出することはできなかった。しかし、この結果から、改良プローブの合成に関する今後の展望を得ることができた。

IVM は様々なイオンチャネルに対して作用を示すことが報告されているが、そのメカニズムについては未だに不明な点も多い。そこで、電気生理学的手法

を用いてイエバエ由来のイオンチャネル (*Musca* GluCl と *Musca* GABACl) に対する IVM の作用について調べた。*Musca* GluCl と *Musca* GABACl に対する IVM の試験は、アフリカツメガエル卵母細胞を用いた TEVC 法で行った。今回、*Musca* GABACl に対して IVM を単独で 3 分間投与することで不可逆的な電流応答が見られた。また、*Musca* GluCl に対してはより高い感受性を示し、EC_{50} を両チャネルで比較すると、GluCl の方が 184 倍高いことがわかった。次に、*Musca* GABACl に対して様々な濃度の GABA を IVM 存在下で投与した。その結果、IVM は EC_{50} より低濃度の GABA の誘起電流を増大し、EC_{50} より高濃度の GABA 誘起電流を阻害することが分かった。そこで EC_5 および EC_{90} のアゴニストを用いて *Musca* GABACl と *Musca* GluCl に対する IVM の増強、阻害作用について調べた。その結果、IVM は両チャネルに対してアゴニストの増強、阻害作用を示した。また、いずれの作用も *Musca* GluCl の方が高い感受性を示し、IVM の主要ターゲットは GluCl であることが示唆された。

GluCl と GABACl の第 3 膜貫通領域の 36'グリシンは、IVM の結合に関与する重要なアミノ酸であることが報告されている。今回、このグリシンをそれぞれアラニンとメチオニンに置換した *Musca* GluCl (G36'M GluCl) および *Musca* GABACl (G36'M GABACl、G36'A GABACl) を作製し、IVM の 3 作用を調べたところ、いずれの作用も消失または減弱した。以上より、IVM の 3 作用は TM1-TM3 の膜貫通ドメインのサブユニット間スペースに結合し、アゴニストの存在あるいは非存在または濃度に依存して作用を示すことがわかった。

以上の本研究結果は、新しい有害生物防除剤の開発についての有用な情報を提供している。